Journal of Nanobiotechnology

RESEARCH

Open Access

Recombinant ferritin-based nanoparticles as neoantigen carriers significantly inhibit tumor growth and metastasis

Wei Zheng[1], Shixiong Li[1], Zhongliang Shi[1], Kailing Su[1], Yu Ding[1], Luyue Zhang[1], Qian Tang[1], Jiani Han[1], Han Zhao[1], Fengwei Wang[2,3], Hongru Zhang[1,4*] and Zhangyong Hong[1,4*]

Abstract

Background Tumor neoantigen peptide-based vaccines, systemic immunotherapies that enhance antitumor immunity by activating and expanding antigen-specific T cells, have achieved remarkable results in the treatment of a variety of solid tumors. However, how to effectively deliver neoantigens to induce robust antitumor immune responses remains a major obstacle.

Results Here, we developed a safe and effective neoantigen peptide delivery system (neoantigen-ferritin nanoparticles, neoantigen-FNs) that successfully achieved effective lymph node targeting and induced robust antitumor immune responses. The genetically engineered self-assembled particles neoantigen-FNs with a size of 12 nm were obtained by fusing a neoantigen with optimized ferritin, which rapidly drainage to and continuously accumulate in lymph nodes. The neoantigen-FNs vaccine induced a greater quantity and quality of antigen-specific $CD8^+$ T cells and resulted in significant growth control of multiple tumors, dramatic inhibition of melanoma metastasis and regression of established tumors. In addition, no obvious toxic side effects were detected in the various models, indicating the high safety of optimized ferritin as a vaccine carrier.

Conclusions Homogeneous and safe neoantigen-FNs could be a very promising system for neoantigen peptide delivery because of their ability to efficiently drainage to lymph nodes and induce efficient antitumor immune responses.

Keywords Tumor neoantigen, Peptide-based vaccine, Vaccine platform, Lymph node-targeting, Ferritin

*Correspondence:
Hongru Zhang
hrzhang@nankai.edu.cn
Zhangyong Hong
hongzy@nankai.edu.cn

Full list of author information is available at the end of the article

Graphical Abstract

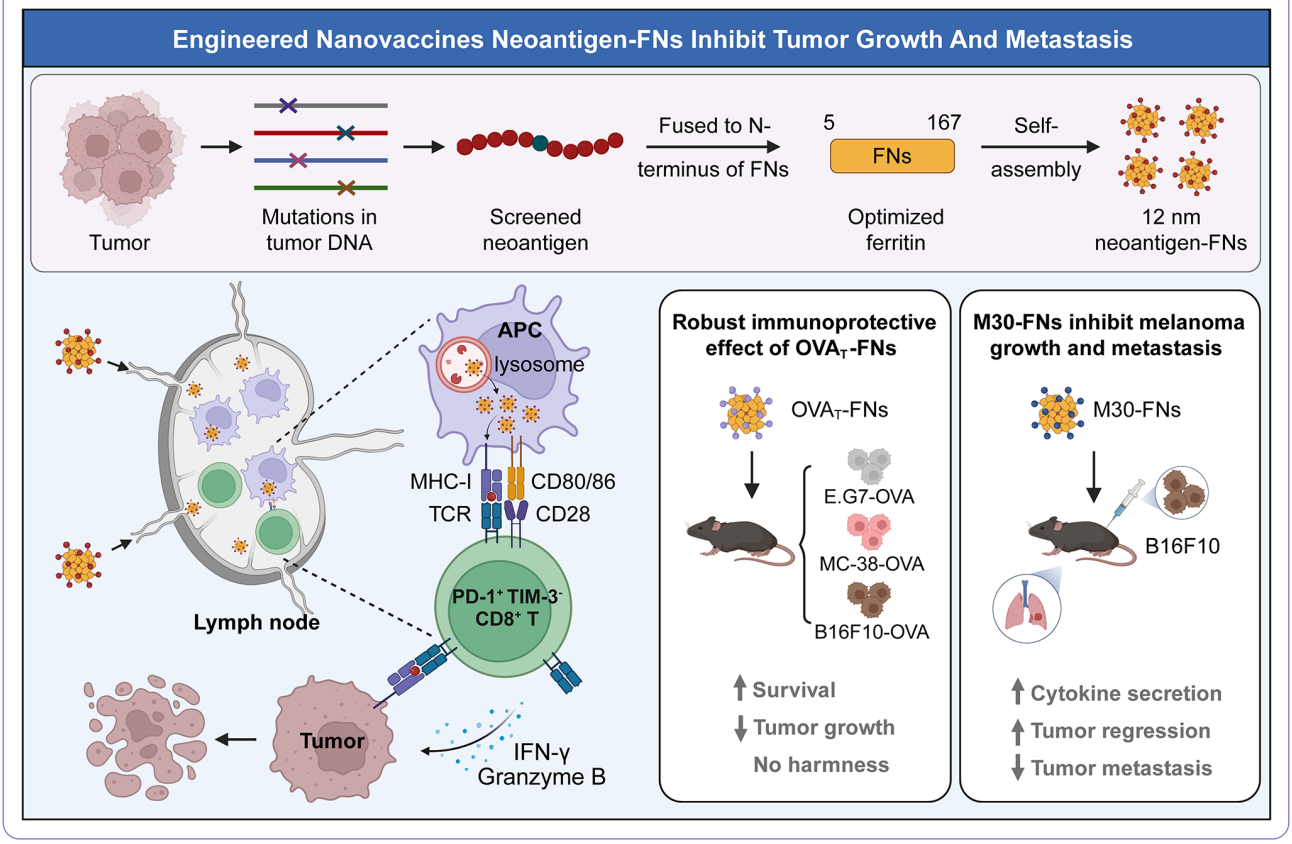

Background

Therapeutic tumor vaccines are personalized immunotherapies that recognize and eliminate malignant cells by stimulating the body to generate tumor antigen-specific $CD8^+$ T cells [1]. Several clinical trials have demonstrated that personalized therapeutic vaccines can significantly prolong the survival of patients with solid tumors [2, 3]. In 2010, the U.S. Food and Drug Administration (FDA) approved Provenge (sipuleucel-T) for the therapy of advanced prostate cancer, suggesting that therapeutic tumor vaccines have promising prospects for the treatment of solid tumors [4, 5].

Advances in rapid genome sequencing technology have driven the development of neoantigen therapeutic vaccines [6–8]. Neoantigens are tumor-specific antigens derived from nonsynonymous mutations and have become ideal targets for therapeutic tumor vaccines because they do not elicit autoimmune responses or central tolerance. Neoantigen peptides have been widely applied in clinical research due to their favorable biosafety, abundant modifiable sites and mature synthetic routes [9, 10]. However, neoantigen peptides usually fail to elicit sufficient antigen-specific cytotoxic T lymphocyte (CTL) responses in vivo because of their lower immunogenicity and poor lymph node-targeted delivery [11, 12]. Therefore, it is imperative to develop an ideal neoantigen peptide delivery system that not only enhances the immunogenicity of neoantigens, but also enables targeted delivery to lymph nodes to stimulate effective antitumor immune responses.

To address these issues, a variety of neoantigen peptide delivery platforms, including polymeric nanoparticles [13], inorganic nanoparticles [14], and liposomes [15], which are able to induce robust CTL responses and significantly inhibit tumor growth in mice, have been developed and validated in preclinical studies. Unfortunately, poor biocompatibility, particle heterogeneity, or inconsistent manufacturing processes have limited the application of these systems in clinical trials [16]. However, protein-caged nanoparticles such as virus-like particles (VLPs) and ferritin family proteins have attracted much attention in drug delivery due to their good biodegradability, highly ordered structures, and simple and repeatable preparation methods [17, 18]. These proteins tend to self-assemble into nanoscale core-shell structures, which would facilitate effective targeting to lymph nodes and persistence in vivo [19]. Tumor peptide vaccines based on VLPs and heat shock proteins have shown strong

efficacy in triggering protective immunity against different tumors [20–22].

Lymph node targeting is often considered critical for the effective delivery in vivo of tumor vaccines and the induction of robust antitumor immune responses [23]. A study comparing the lymph node-targeting ability of four different protein-caged nanoparticles demonstrated that engineered human ferritin heavy chain (hFTN) nanoparticles have greater potential for direct lymph node targeting and tumor immunotherapy [24]. Ferritin is a 12 nm spherical particle self-assembled from 24 monomers with the advantages of nanoscale size [25], multiple peptide modification sites, good biocompatibility, and thermal stability [26]. In addition, ferritin has been extensively investigated for the delivery of viral antigens such as influenza and SARS-CoV-2 antigens [27–32], and several clinical studies have shown that ferritin has excellent biosafety as an antigen delivery vehicle [33, 34]. However, studies on ferritin as a delivery platform for neoantigen peptides in tumor vaccines have been very limited [35–37]. Therefore, we expect to develop a ferritin-based tumor vaccine platform for the delivery of neoantigen peptides to enhance antitumor immune responses.

In this study, *Helicobacter pylori*-derived ferritin [25], which is distantly related to human evolution, was chosen as a delivery platform for tumor neoantigen peptides due to its advantage to prevent the generation of autoimmune responses or immune tolerance [38]. The results showed that OVA_T-ferritin nanoparticles (OVA_T-FNs) are homogeneous and stable 12 nm particles and have significantly greater immunogenicity than OVA_T free peptides. Moreover, OVA_T-FNs can rapidly drainage to lymph nodes and reside for a long time to enhance uptake by antigen-presenting cells (APCs) in lymph nodes. Effective antigen-specific immune responses were induced by OVA_T-FNs + Poly(I: C) in vivo, resulting in significant inhibition of tumor growth and metastasis. In addition, OVA_T-FNs possessed excellent biosafety, which will facilitate subsequent clinical translation.

Methods

Mice

Female wild-type (WT) C57BL/6 and BALB/c mice were purchased from Beijing Vital River Laboratory Animal Technology Co., Ltd. (Beijing, China), and female OT-1 transgenic mice were purchased from The Jackson Laboratory. All mice used in this study were between 6 and 8 weeks old and were maintained under specific pathogen-free conditions in the animal facility at Nankai University. All mice were housed in groups of 5 under conditions of a 12-hour light-dark cycle (8:00–20:00, light; 20:00–8:00, dark), constant room temperature (21 °C), suitable humidity (40%~60%), and free access to food and water. The animal procedures were performed with ethical compliance and approval from the Institutional Animal Care and Use Committee at Nankai University.

Cell lines

The E.G7-OVA, MC-38-OVA, B16F10, 3T3, and LO2 cell lines were purchased from American Type Culture Collection (ATCC, Manassas, VA, USA). The B16F10-OVA cells were a gift from Prof. Song Zhang's lab. The E.G7-OVA, MC-38-OVA, B16F10-OVA, and B16F10 cells were grown in RPMI 1640 (Gibco, CA, USA) supplemented with 10% fetal bovine serum (FBS, Biological Industries) and 1% penicillin-streptomycin (NCM Biotech, Cat. #C100C5). In addition, 50 μM 2-mercaptoethanol (Aladdin, Cat. #M301574) and 0.4 mg/mL G-418 (Solarbio, Cat. #IG0010) were used for the culture of E.G7-OVA cells, and 1.5 μg/mL puromycin (Solarbio, Cat. # P8230) was used for the culture of MC-38-OVA cells to exclude cells not overexpressing OVA. The 3T3 and LO2 cells were grown in DMEM (Gibco, CA, USA) supplemented with 10% FBS and 1% penicillin-streptomycin. All cells tested negative for mycoplasma contamination according to the ATCC Universal Mycoplasma Detection Kit (ATCC, Cat. #30–1012 K) and were cultured at 37 °C in a humidified incubator with 5% CO_2.

Protein biosynthesis and purification

The gene encoding *Helicobacter pylori* ferritin (residues 5-167) was codon-optimized to adapt to the *Escherichia coli* (*E. coli*) expression system, and a point mutation (Asn19Gly) was designed to remove a potential N-linked glycosylation site. The OVA_T peptide (SIINFEKL) followed by a $(GGS)_3$ linker and the M30 peptide (PSKPSFQEFVDWENVSPELNSTDQPFL) followed by a SASGG linker were fused to the N-terminus of ferritin (residues 5-167) to generate OVA_T-FNs and M30-FNs, respectively [7]. Moreover, FNs without peptides at the N-terminus of ferritin (residues 5-167) were prepared as a control. The constructs were cloned and inserted into the pET-28a (+) expression vector (Novagen, Madison, WI, USA) using the NcoI and XhoI restriction sites. The recombinant plasmids were transformed into *E. coli* BL21(DE3) competent cells (ZOMANBIO, Cat. #ZK201), and the bacterial cells were grown in LB media supplemented with 50 μg/mL kanamycin (Solarbio, Cat. #K8020) at 37 °C until an absorbance of 0.6 was reached at 600 nm. The proteins were induced to be overexpressed by 0.7 mM isopropyl β-D-1-thiogalactopyranoside (IPTG) (Solarbio, Cat. #II0130) for 16 h at 16 °C.

The bacterial cells were harvested and resuspended in lysis buffer (50 mM Tris, 500 mM NaCl, 5% glycerol, pH 8.0) and then homogenized at a pressure of 700 bar. The supernatant containing the recombinant proteins was obtained by centrifugation at 18,000 rpm for 40 min at 4 °C, and the proteins were isolated by Ni-nitrilotriacetic

acid affinity chromatography. Briefly, 2 mL of Ni-NTA resin (TransGen, Cat. #DP101) was used to purify proteins, which were then equilibrated with PBS (pH 7.2 ~ 7.4) and incubated with the supernatant for 2 times. Nontarget proteins were removed by washing with 10 mM, 50 mM, or 100 mM imidazole, and target proteins were eluted with 300 mM imidazole. The size and purity of the harvested proteins were determined by SDS-PAGE. The eluted proteins were buffer exchanged into PBS (pH 7.2 ~ 7.4) containing 1 mM EDTA (Solarbio, Cat. #E1170) and 5% glycerol and concentrated to less than 5 mL using Amicon-Ultra15 centrifugal filters (EMD Millipore) with a 100-kDa molecular weight cutoff (MWCO). The concentrated proteins were further purified by size exclusion chromatography using a HiPrep 16/60 Sephacryl S-500 h size-exclusion column in the above buffer at a flow rate of 0.8 mL/min. The purified proteins were concentrated to 2.5 mg/mL using Amicon-Ultra15 centrifugal filters with a 100-kDa MWCO after removal of endotoxin according to the manufacturer's protocols (Thermo, Cat. #88272), and then 5% glycerol was added, followed by storage at -80 °C.

Negative-stain electron microscopy

For the negative-staining study, 4 μL of 100 μg/mL protein sample was applied to a carbon film-coated 300-mesh Cu grid (Beijing Zhongjingkeyi Technology Co., Ltd., Beijing, China) for 1 min. After air-drying, the sample was negatively stained with 1% (w/v) uranyl acetate for 1 min and then observed by transmission electron microscopy (TEM) (QUANTA 200, FEI company, USA) operating at 100.0 KV.

Dynamic light scattering (DLS) and zeta potential analysis

Particle size and zeta potential analysis of FNs and OVA_T-FNs at a concentration of approximately 2 mg/mL were performed using a Zetasizer Nano ZS (Malvern Instruments Ltd., UK).

Blood and tissue processing

Approximately 150 μL of peripheral blood was collected into a 1.5 mL EP tube containing 30 μL of 0.5 M EDTA, and 1.5 mL of ACK buffer (Solarbio, Cat. #R1010) was added to lyse red blood cells twice for 5 min each. Lymph nodes or spleen placed between two 40 μm filters were mechanically prepared into single cells in a 12-well plate containing 1 mL of MACS buffer (1×PBS containing 0.5% BSA and 2 mM EDTA). In addition, the splenocytes were lysed at room temperature for 5 min with 2 mL of ACK buffer to remove red blood cells. The obtained single-cell suspension was filtered through a 40 μm nylon mesh filter for subsequent flow cytometry detection or transfer experiments.

Preparation of bone marrow-derived dendritic cells (BMDCs)

Bone marrow was flushed from the femurs and tibias of C57BL/6 mice with ice-cold RPMI 1640 medium containing 2% penicillin-streptomycin. Red blood cells were lysed, and the remaining cells were seeded in a 10 cm tissue culture dish containing 12 mL of BMDC medium consisting of RPMI 1640 medium supplemented with 10% heat-inactivated fetal bovine serum (HI-FBS), 1% penicillin-streptomycin, 50 μM 2-mercaptoethanol, 20 ng/mL IL-4 (PeproTech, Cat. #214−14) and 40 ng/mL GM-CSF (PeproTech, Cat. #315-03). On day 2, nonadherent and loosely adherent cells were collected and transferred to a new culture dish, after which 4 mL of fresh BMDC medium was added. On day 4, half of the medium was gently removed, and an equal volume of fresh medium was added. On day 6, BMDCs were identified by flow cytometry and used for subsequent experiments.

In vitro cellular uptake assay

First, suitable cells cover glasses (NEST, Cat. #801010) were placed in a 24-well plate and 5×10^5 immature BMDCs obtained as described above were added and cultured for 24 h. BMDCs were then incubated with 2 nmol Cy5-labeled OVA_T, FNs or OVA_T-FNs for 4 h. After the unphagocytosed vaccines were washed away with PBS, the BMDCs were stained with CD11c-FITC antibody at 4 °C for 30 min, followed by fixation with 200 μL of 1% paraformaldehyde (Solarbio, Cat. #P1111) at 4 °C for 20 min. The cover glasses were harvested and stained with DAPI, after which the localization of Cy5-labeled antigen in FITC-positive cells was detected by confocal laser scanning microscopy (CLSM; TCS SP5, Leica, Germany).

Evaluation of endosomal escape ability

A total of 1×10^6 immature BMDCs were grown in 35 mm confocal dishes (NEST, Cat. #801001) for 24 h. Then, 2 nmol of FITC-labeled OVA_T, FNs or OVA_T-FNs were added and cocultured for 4 h. After being washed 5 times with PBS, the BMDCs were stained with LysoTracker (Invitrogen, Waltham, MA, USA, Cat. #L7528) for 1 h, followed by Hoechst (US Everbright, Cat. #H4078) for 30 min. The colocalization of FITC and LysoTracker was detected by confocal laser scanning microscopy (CLSM; TCS SP5, Leica, Germany) to analyze the endosomal escape ability of FNs and OVA_T-FNs.

Activation and maturation of BMDCs and cross-presentation of OVAT peptide

The cells and culture supernatant were harvested after 1×10^6 BMDCs were cocultured with 2 nmol of OVA_T, FNs or OVA_T-FNs for 24 h. BMDCs were then stained with CD80, CD86, MHC-I, MHC-II, CD40, and

SIINFEKL-H2Kb antibodies for 30 min at 4 °C, and the frequencies of activation markers were analyzed with a BD FACSCalibur Flow Cytometer (BD Biosciences, San Jose, CA, USA). The concentrations of IL-12 (P70), IFN-α1, IL-6, IFN-γ and TNF-α in the culture supernatant were determined by enzyme-linked immunosorbent assay (ELISA) according to the manufacturer's protocols.

In vivo imaging and lymph node targeting

BALB/c or C57BL/6 mice were immunized with PBS, 6 nmol Cy5-labeled OVA_T, FNs, or OVA_T-FNs in the groin. The fluorescence intensities at the injection site, isolated lymph nodes and various organs were analyzed 24, 48, and 72 h after immunization using an IVIS Lumina imaging system (IVIS Lumina II, Xenogen, USA).

Antigen uptake and activation of APCs in lymph nodes

C57BL/6 mice were immunized in the groin with Cy5-labeled OVA_T, FNs or OVA_T-FNs at a dose of 6 nmol per side. Twenty-four hours after immunization, the lymph nodes were harvested and prepared into single-cell suspensions. Then, the frequencies of Cy5 in APCs, such as DCs ($CD11c^+$), macrophages ($CD11b^+$ $F4/80^+$), and B cells ($B220^+$), as well as the frequency of activated DCs ($CD80^+$ $CD86^+$ $CD11c^+$), were analyzed by flow cytometry.

In vivo proliferation assay

Splenocytes from OT-1 mice were labeled with 5 μM CFSE (Invitrogen, Cat. #65–0850) for 1 h at 37 °C and then transferred intravenously to C57BL/6 mice, which were then immunized subcutaneously in the groin with 6 nmol of OVA_T, FNs and OVA_T-FNs in the presence or absence of 50 μg of Poly(I: C) (InvivoGen, Cat. #tlrl-pic-5) 24 h after transfer. The attenuation of CFSE fluorescence intensity of OVA_T-specific $CD8^+$ T cells in the spleen was analyzed by flow cytometry at 24, 48, and 72 h after immunization. The proliferation index, representing the total number of divisions / cells that went into division, was calculated using the Proliferation Tool in FlowJo v10.8.1 software.

In vivo target cell lysis assay

Splenocytes from C57BL/6 mice were resuspended in RPMI-1640 medium supplemented with 1% penicillin-streptomycin, and 50 μM 2-mercaptoethanol, and the cell concentration was adjusted to 1×10^7 cells/mL [39]. The above cells were divided into two aliquots, one of which was labeled with OVA_T peptide at a final concentration of 25 μM for 2 h at 37 °C, while the other was unlabeled. Splenocytes loaded with OVA_T peptide and unloaded with OVA_T peptide were labeled with 5 μM and 0.5 μM CFSE, respectively, for 1 h at 37 °C. The cells were washed twice with PBS to remove unbound CFSE dye and subsequently mixed at a ratio of 1:1 after adjusting the cell concentration to 5×10^7 with PBS. Additional C57BL/6 mice without any treatment were immunized with PBS, OVA_T, OVA_T+Poly(I: C), OVA_T-FNs, or OVA_T-FNs + Poly(I: C). A total of 7×10^6 mixed cells were injected intravenously into mice immunized for 8 days at a dose of 200 μL per mouse. Eighteen hours after injection, single-cell suspensions of the spleens and lymph nodes were prepared, and the frequencies of splenocytes labeled with high and low concentrations of CFSE were analyzed by flow cytometry. The specific lysis percentage was calculated according to the published formula [22]:

$$\%\,\text{specific lysis} = \frac{\text{CFSE}^{\text{low}} \times \alpha - \text{CFSE}^{\text{high}}}{\text{CFSE}^{\text{low}} \times \alpha}$$

$$\alpha = \text{ratio of transferred CFSE}^{\text{high}} \text{ to CFSE}^{\text{low}} \text{ cell counts}$$

Immunizations

A total of 6 nmol of OVA_T, M30, FNs, OVA_T-FNs, or M30-FNs alone, or prepared by mixing with 50 μg of Poly(I: C) were formulated in 100 μL of PBS and immunized subcutaneously via the groin.

Enzyme-linked immunospot (ELISpot) assay

ELISpot plates (EMD Millipore, MSIPS4510) were pretreated with 50 μL of 35% ethanol for 30 s and washed 5 times with sterile water before being coated with 100 μL of 15 μg/mL anti-IFN-γ (MABTECH, Cat. #3321–2 A) overnight at 4 °C. After coating, the antibody was discarded, and the plate was blocked for 1 h with complete medium (RPMI-1640 supplemented with 10% FBS and 1% penicillin-streptomycin). A total of 2×10^5 splenocytes were added to each well and restimulated for 48 h at 37 °C with complete medium containing OVA_T or M30 peptide at a final concentration of 10 μg/mL. The cells were washed away, and the plates were incubated with 100 μL of 1 μg/mL biotinylated detection antibody (MABTECH, Cat. #3321–2 A) for 2 h at room temperature. The plate was washed 5 times with PBS and incubated with streptavidin-ALP (MABTECH, Cat. #3321–2 A) diluted at a ratio of 1:1000 for 1 h at room temperature. After washing with PBS 5 times, 100 μL of the substrate NBT&BCIP (Sangon Biotech, Cat. #C510032) prepared with 1× color development buffer was added to each well until obvious spots appeared, after which the reaction was stopped with 200 μL of ddH_2O. After dying, the spots were counted with an ELISpot reader (AID iSpot, AID-Autoimmune Diagnostika GmbH, Strassberg, Germany).

Experiments to detect immune responses induced by vaccines

C57BL/6 mice were immunized on days 0 and 14, and the peripheral blood and spleen were collected on day 21 to analyze vaccine-induced immune responses. The frequencies of OVA_T-specific $CD8^+$ T cells in the peripheral blood and spleen were measured by flow cytometry. The phenotypes of $CD8^+$ T cells in peripheral blood were evaluated by flow cytometry analysis of the proportions of PD-1^+ TIM-3^- cells, effector memory T (Tem) cells, and central memory T (Tcm) cells. Vaccine-induced CTL responses were measured by the secretion of IFN-γ, TNF-α, or Granzyme B by $CD8^+$ T cells.

Prophylactic, therapeutic and metastasis model experiments

For prophylactic model experiments, C57BL/6 mice were immunized on days 0, 14 and 28. Fourteen days after the third immunization, 5×10^5 E.G7-OVA, 1×10^6 MC-38-OVA, or 3×10^5 B16F10-OVA cells in 100 μL of PBS were subcutaneously implanted into the right flank of each mouse.

For metastasis model experiments, C57BL/6 mice were immunized on days 0, 14 and 28, 1×10^5 B16F10 cells in 200 μl of PBS were injected through the tail vein on day 35, and the lungs of the mice were removed on day 57 to count the number of metastatic foci.

For therapeutic model experiments, C57BL/6 mice were subcutaneously implanted in the right flank with 1×10^5 B16F10 cells in 100 μL of PBS on day 0 and then immunized three times on days 5, 8, and 12.

The tumor volume was estimated by the following formula: tumor volume = length × $width^2\times0.5$. Animals were euthanized when the tumor reached 1.5 cm in diameter or surpassed 1500 mm^3 in volume or when significant weight loss was observed.

ELISA

The culture medium supernatant of BMDCs cocultured with vaccines and of splenocytes restimulated with OVA_T peptide were collected, and the concentrations of cytokines were detected by ELISA kits (BioLegend, San Diego, CA, USA). The concentrations of IL-12(p70) (Cat. #433604), IFN-α1 (Cat. #447904), TNF-α (Cat. #430904), IFN-γ (Cat. #430804), and IL-6 (Cat. #431304) were detected according to the manufacturer's protocols.

Flow cytometry analysis

For the APCs uptake analysis, cells were preincubated with 0.25 μg of TruStain FcX™ PLUS anti-mouse CD16/32 blocking antibody (BioLegend, clone. S17011E) per 10^6 cells in a volume of 100 μl for 10 min on ice to reduce nonspecific binding. After FcR blocking, the cells were then stained for 30 min at 4 °C with surface antibodies diluted at 1:300 in 100 μL of FACS buffer (fluorochrome-conjugated antibodies purchased from BioLegend unless otherwise indicated): CD45 (Cat. #103133. clone. 30-F11), CD11b (Cat. #101292. clone. M1/70), CD11c (Cat. #117306 and 117307. clone. N418), CD11c (BD Biosciences, Cat. #612797, clone. HL3), CD80 (Cat. #104705. clone. 16-10A1), CD86 (Cat. #105025. clone. GL-1), CD40 (Cat. #157506. clone. FGK45), MHC-I (Cat. #114612. clone. 28-8-6), MHC-II (Cat. #107625. clone. M5/114.15.2), B220 (Cat. #103205. clone. RA3-6B2), F4/80 (Cat. #123110. clone. BM8), and SIINFEKL-H2Kb (Cat. #141605. clone. 25-D1.16). After staining, the cells were washed once with FACS buffer and resuspended in 300 μL of PBS for flow cytometry detection.

For T-cell tetramer analysis, single cells derived from the peripheral blood or spleen were first incubated with 100 μL of PBS containing 50 nM dasatinib (MACKLIN, Cat. #D828602) for 30 min at room temperature. The samples were washed once and treated with an anti-CD16/32 antibody for 10 min on ice. The cells were then stained with tetramer antibody (MBL, Cat. #TS-5001–1 C) diluted 1:20 in 50 μL of FACS buffer containing 50 nM dasatinib for 45 min at 4 °C under light protection. After washing once with FACS buffer, the cells were stained with surface antibodies diluted at 1:300 in 100 μL of FACS buffer (fluorochrome-conjugated antibodies purchased from BioLegend unless otherwise indicated) for 30 min at 4 °C: CD8 (GeneTex, Cat. #GTX76348. clone. KT15), PD-1 (Cat. #135209. clone. 29 F.1A12), TIM-3 (Cat. #119718. clone. RMT3-23), CD44 (Cat. #103043. clone. IM7), and CD62L (BD Biosciences, Cat. #564109, clone. MEL-14).

For intracellular cytokine analysis, 1×10^6 splenocytes were first stimulated with 10 μg/mL OVA_T peptide and Golgi plug (BD Biosciences, Cat. #555029) at 37 °C for 6 h. The cells were then treated with an anti-CD16/32 blocking antibody at 4 °C for 10 min and subsequently stained with CD3 (BD Biosciences, Cat. #564379, clone. 145-2C11), CD4 (Cat. #100491. clone. GK1.5) and CD8 (Cat. #100706. clone. 53−6.7) diluted at 1:300 for 30 min at 4 °C. The cells were washed once with FACS buffer and fixed and permeabilized at 4 °C for 1 h using the FoxP3/Transcription Factor Staining Buffer Set (Invitrogen, Cat. #00-5523-00). The cells were washed once with 1× wash buffer and then stained with the following intracellular antibodies: IFN-γ (Cat. #505808. clone. XMG1.2), TNF-α (Cat. #506313. clone. MP6-XT22), and Granzyme B (Cat. #372216. clone. QA16A02) diluted at 1:300 in 50 μL PBS at 4 °C overnight. The cells were washed twice with PBS and prepared for flow cytometry detection.

The cells were acquired on a BD FACSCalibur Flow Cytometer (BD Biosciences, San Jose, CA, USA) or a BD LSRFortessa X-20 (BD Biosciences) using BD FACSDiva

Software v8.0.3 (BD Biosciences). All collected data were analyzed with FlowJo version V10.8.1.

CCK-8 assay

The 3T3 cells (5×10^3), LO2 cells (5×10^3), and PBMCs (1×10^4) were seeded into 96-well plates and cultured for 24 h. Then, the cells were treated with different doses of FNs and OVA_T-FNs for additional 24 h. After treatment, CCK-8 solution (NCM Biotech, Cat. #C6005) was added to each well and incubated for 2.5 h. The absorbance was then measured at 450 nm and 600 nm using a Cell Imaging Multi-Mode Reader (Cytation 5, BioTek, Winooski, VT, USA).

Hematoxylin and eosin (H&E) staining and determination of various enzymes in serum

Fourteen days after the third immunization, 200 μL of peripheral blood was collected and placed at 4 °C overnight, followed by centrifugation at 1,000 rpm for 20 min to harvest the serum. The heart, liver, spleen, lung and kidney were removed and fixed in 15 mL of 4% paraformaldehyde (Solarbio, Cat. #P1110) for 4 days. Organ damage and the serum concentrations of aspartate aminotransferase (AST), alanine aminotransferase (ALT), blood urea nitrogen (BUN) and creatinine (CRE) were determined by Tianjin JingNuo Pathological Diagnostic Co.

Statistical analyses

Statistical analyses were performed using GraphPad Prism 8.0.2 software. All results were presented as the mean±s.e.m. An unpaired Student's *t* test, one-way ANOVA with Tukey's multiple-comparison test, two-way ANOVA with Tukey's multiple-comparison test or log rank test was used for comparisons between the groups. *P* values less than 0.05 were considered to indicate statistical significance. No sample in any representative experiment was excluded from the analysis.

Results

Engineering and characterization of OVAT-FNs tumor vaccines

The homogeneity, biocompatibility, and size of tumor vaccines are critical to their effectiveness in suppressing tumors [40]. We expect to develop a more effective and safer peptide delivery platform for tumor neoantigens relying on *Helicobacter pylori*-derived ferritin nanoparticles. SIINFEKL (OVA_T) was fused to optimized ferritin proteins to prepare OVA_T-FNs, in which the first four amino acids at the N-terminus were omitted because the fifth amino acid is better displayed on the particle surface, and an N19Q mutation was introduced to abolish a potential N-linked glycosylation site (Fig. 1a) [27].

To test whether the OVA_T-FNs protein subunits could be synthesized in an *E. coli* expression system and subsequently self-assembled into nanoparticles, we investigated the purity, structural integrity, and size of the obtained OVA_T-FNs. SDS-PAGE of purified FNs and OVA_T-FNs revealed a single protein band corresponding to the protein subunit (Fig. 1b). The peak shape of OVA_T-FNs analyzed by molecular exclusion chromatography was similar to that of FNs, suggesting that the fusion of OVA_T peptide at the N-terminus of FNs did not affect the self-assembly of the optimized ferritin into nanoparticles (Fig. 1c). OVA_T-FNs were homogeneous 12 nm spherical particles similar to the native structure, as revealed by TEM and DLS (Fig. 1d, e). Moreover, the particle size of OVA_T-FNs was not affected after treatment at 4 °C for 7 days or 65 °C for 10 min, suggesting that OVA_T-FNs are able to tolerate high temperatures and have good stability, which is important for the clinical translation of these vaccines (Fig. S1). In addition, the absolute zeta potentials of FNs and OVA_T-FNs were approximately 10 mV and 8 mV, respectively, indicating that the individual particles were well dispersed and stable (Fig. 1f). Together, these data suggested that OVA_T-FNs prepared by fusion expression have superior purity, a uniform particle size, and good thermal stability.

Activation and cross-presentation of BMDCs after the uptake of OVAT-FNs

To demonstrate that optimized ferritin can be used as a tumor vaccine vector, we first investigated whether OVA_T-FNs could be taken up by BMDCs, the most effective APCs for initiating naïve $CD8^+$ T cells, and efficiently cross-present OVA_T peptides on the cell surface. Fluorescence confocal microscopy images showed that the uptake of OVA_T-FNs by $CD11c^+$ BMDCs was dramatically greater than that of free OVA_T after coincubation with BMDCs for 4 h (Fig. 2a) and the uptake of OVA_T-FNs by BMDCs significantly increased with prolonged coculture time (Fig. S2a). Moreover, FNs and OVA_T-FNs could also be taken up by $CD11b^+$ BMDMs (Fig. S2b). In addition, OVA_T-FNs did not fully colocalize with lysosomes but were predominantly localized in the cytoplasm (Fig. 2b), suggesting that OVA_T-FNs can escape from lysosomes into the cytoplasm and be degraded by the proteasome into peptide fragments. The maturation of BMDCs plays an essential role in triggering tumor-specific CTL responses [41]. The expression of the surface activation markers CD80, CD86, MHC-I, MHC-II, and CD40 was significantly upregulated in BMDCs after coculture with OVA_T-FNs, indicating that OVA_T-FNs induced the activation of BMDCs (Fig. 2c-g and Fig. S3). The frequency of SIINFEKL-$H2Kb^+$ on the surface of BMDCs was analyzed by flow cytometry to verify whether BMDCs cross-present OVA_T antigen via MHC-I

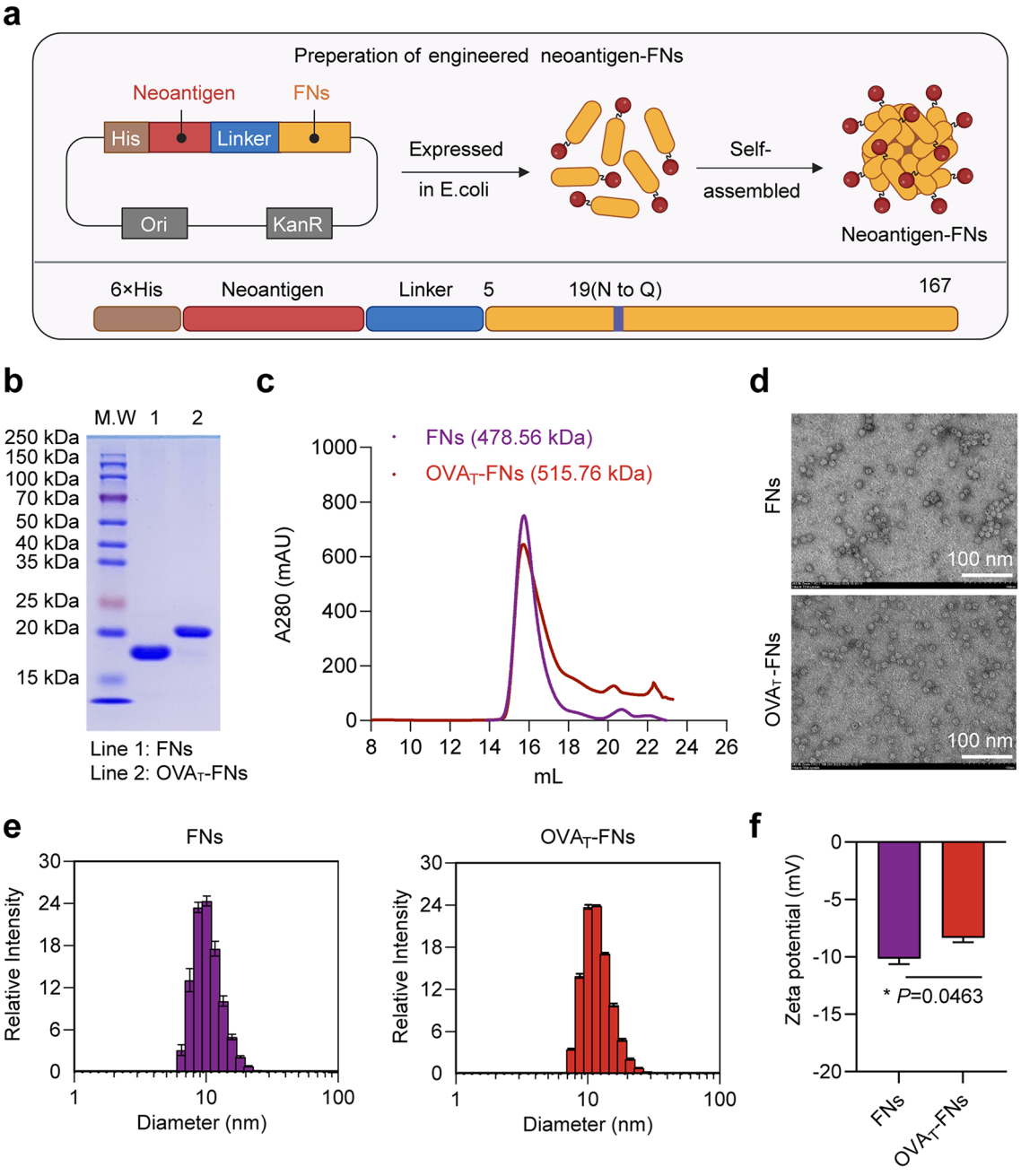

Fig. 1 Design and characterization of neoantigen-FNs. **a**, Schematic diagram of the design of neoantigen-FNs. **b**, SDS-PAGE analysis of purified FNs (monomer ~ 19.94 kDa) and OVA$_T$-FNs (monomer ~ 21.49 kDa). **c**, Size exclusion chromatography analysis of purified FNs and OVA$_T$-FNs. The proteins formed ~ 478.56 kDa (FNs) and ~ 515.76 kDa (OVA$_T$-FNs) nanoparticles. **d**, TEM images of FNs (top) and OVA$_T$-FNs (bottom) stained with 1% uranyl acetate. Scale bar, 100 nm. **e**, DLS measurements of FNs (left) and OVA$_T$-FNs (right)($n = 3$). **f**, Zeta potential measurements of FNs and OVA$_T$-FNs. The mean zeta potentials were − 10 mV and − 8 mV for FNs and OVA$_T$-FNs, respectively($n = 3$). **e**, **f**, Data are presented as the mean ± s.e.m. **f**, The statistical significance of differences between the groups was assessed using two-tailed unpaired Student's *t* test. *$P < 0.05$, **$P < 0.01$, ***$P < 0.001$, ****$P < 0.0001$

molecules, and the results showed that 10% of BMDCs cocultured with OVA$_T$-FNs were able to cross-present SIINFEKL to the cell surface through MHC-I (Fig. 2h and Fig. S3).

In addition, cytokines secreted by mature BMDCs are also critical for downstream immune activation [42]. IL-12(p70) acts as a polarizing factor that promotes the differentiation of naive CD4$^+$ T cells to T helper 1 (Th1) cells and mediates an effective adaptive immune response [43]. The concentrations of cytokines in the culture supernatant of BMDCs cocultured with OVA$_T$-FNs for 24 h were determined by ELISA, and the results showed that the concentrations of IL-12(p70), IFN-α1, IL-6, IFN-γ and TNF-α were significantly increased (Fig. 2i,

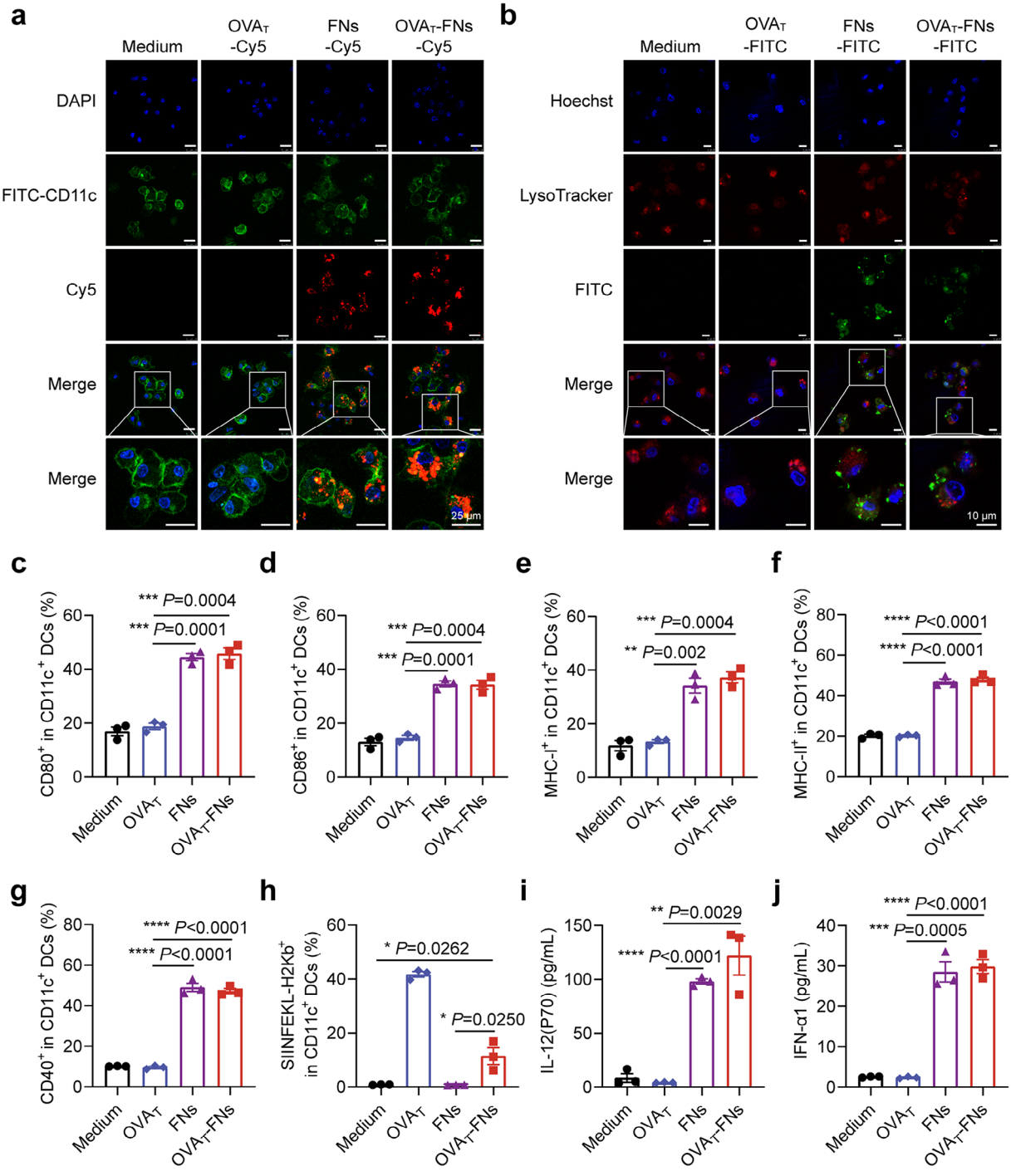

Fig. 2 The uptake of OVA $_T$-FNs by BMDCs induced their activation and maturation in vitro. **a**, **b**, OVA$_T$-FNs were taken up by BMDCs and escaped from lysosomes into the cytoplasm. **a**, Confocal fluorescence images of BMDCs treated with OVA$_T$-Cy5 (red), FNs-Cy5 (red), or OVA$_T$-FNs-Cy5 (red) for 4 h. The nuclei and surface markers of BMDCs were stained with DAPI (blue) and a FITC-conjugated CD11c antibody (green), respectively. Scale bar, 25 μm. **b**, Confocal fluorescence images of BMDCs treated with OVA$_T$-FITC (green), FNs-FITC (green), or OVA$_T$-FNs-FITC (green) for 4 h. The nuclei and lysosomes of BMDCs were stained with Hoechst (blue) and LysoTracker (red), respectively. Scale bar, 10 μm. **c**-**g**, Activation of BMDCs induced by OVA$_T$-FNs. Flow cytometry analysis of the frequencies of CD80$^+$ (**c**), CD86$^+$ (**d**), MHC-I$^+$ (**e**), MHC-II$^+$ (**f**), and CD40$^+$ (**g**) cells in CD11c$^+$ BMDCs treated with OVA$_T$, FNs, or OVA$_T$-FNs for 24 h ($n=3$). **h**, Cross-presentation efficiency was characterized by flow cytometry analysis of the frequency of SIINFEKL-H2Kb$^+$ cells among CD11c$^+$ BMDCs ($n=3$). **i**, **j**, ELISA analysis of IL-12(P70) (**i**) and IFN-α1 (**j**) in the culture supernatant of BMDCs after treatment with OVA$_T$, FNs, or OVA$_T$-FNs for 24 h ($n=3$). **c**-**j**, Data are presented as the mean ± s.e.m. Statistical significance between the groups was assessed using two-tailed unpaired Student's *t* test. *$P<0.05$, **$P<0.01$, ***$P<0.001$, ****$P<0.0001$

j and Fig. S4). Together, these results confirmed that OVA_T-FNs can be taken up by APCs, induce APCs activation and maturation, and enhance antigen presentation via MHC-I.

In vivo targeting and activation of APCs in lymph nodes by OVA_T-FNs

The effective delivery of tumor vaccines to lymph nodes and the maturation and cross-presentation of APCs in vivo are critical for triggering powerful antitumor responses [44, 45]. Therefore, we investigated whether OVA_T-FNs can drainage to lymph nodes and be taken up by APCs. Live fluorescence images revealed highly distinct Cy5 fluorescence in the groin of mice immunized with OVA_T-FNs at 24, 48, and 72 h after immunization, suggesting that compared with free OVA_T, OVA_T-FNs could persist at the injection site (Fig. 3a, b).

Next, we isolated various tissues of immunized mice to examine the biodistribution of OVA_T-FNs and whether they could localize to lymph nodes. Consistent with the results shown in Fig. 3a, b, remarkable localization of OVA_T-FNs was detected in the lymph nodes at 24 h and even 72 h after immunization, suggesting that OVA_T-FNs can effectively target the lymph nodes (Fig. 3c, d). Among the remaining organs, Cy5 fluorescence could be detected only in the liver and kidney at 24 h post injection, which might be related to the metabolic function of the liver and kidney as normal metabolic organs (Fig. S5a, b). In addition, the lymph nodes of FNs or OVA_T-FNs-treated mice were significantly swollen 24 h after immunization and flow cytometry data showed the number of various of immune cells were increased compared with the other groups. However, OVA_T-specific $CD8^+$ T cells had not been dramatically expanded in any of the groups (Fig. S5c). The above results suggest that OVA_T-FNs can be retained in vivo for a long time and can rapidly distribute to lymph nodes. Prolonged retention of OVA_T-FNs in lymph nodes would facilitate their uptake by APCs and infiltration of other immune cells.

To verify whether OVA_T-FNs can be taken up by APCs in lymph nodes. C57BL/6 mice were injected subcutaneously with Cy5-labeled OVA_T-FNs, and the single-cell suspension of lymph nodes were prepared 24 h later. The frequencies of $Cy5^+$ in $CD11c^+$ DCs, macrophages, and B cells were significantly increased in OVA_T-FNs-treated group, but these cells largely did not take up free OVA_T peptide (Fig. 3e-g). Moreover, immunization with OVA_T-FNs resulted in a significant increase in the frequency of the activation marker $CD80^+$ $CD86^+$ in $CD11c^+$ DCs compared to that in cells immunized with OVA_T free peptides (Fig. 3h). These results suggest that OVA_T-FNs can drainage to lymph nodes, reside there for long periods of time. This may provide an opportunity for APCs to continuously take up OVA_T-FNs and come into full contact with T cells.

Triggering and expansion of OVAT-specific CD8+ T cells induced by OVAT-FNs

The ability to induce the production and activation of antigen-specific $CD8^+$ T cells is an important criterion for evaluating the efficacy of tumor vaccines. First, we investigated whether OVA_T-FNs could induce the proliferation of OVA_T-specific $CD8^+$ T cells.

In vitro, CFSE-labeled $CD8^+$ T cells isolated from OT-1 mice were co-cultured with vaccine-treated BMDCs for 4 days, and then the fluorescence intensity of CFSE was measured by flow cytometry (Fig. S6a). The results suggested OVA_T-specific $CD8^+$ T cells cocultured with OVA_T-FNs-treated BMDCs showed more pronounced attenuation of CFSE fluorescence and a higher proliferative index, and most of the cells had divided for 1–5 generations. In contrast, no significant attenuation of CFSE fluorescence intensity was detected in the OVA_T-treated group (Fig. S6b-d).

Since almost all peptide vaccines currently in clinical trials require adjuvants to enhance their induced immune responses [10, 46], consistent with previous studies, we also included Poly(I: C) as an adjuvant in all of our in vivo experiments.

In the in vivo proliferation assay, although the proliferation of OVA_T-specific $CD8^+$ T cells induced by OVA_T-FNs + Poly(I: C) was delayed compared to OVA_T+Poly(I: C), because OVA_T-FNs need to be taken up by APCs for antigen presentation (Fig. S7a). However, 72 h after immunization, the percentage of OVA_T-specific $CD8^+$ T cells was significantly elevated in the spleen of mice immunized with OVA_T-FNs + Poly(I: C) than with OVA_T+Poly(I: C) (Fig. S7b). Moreover, compared to OVA_T+Poly(I: C), OVA_T-FNs + Poly(I: C) induced a more significant decrease in CFSE fluorescence intensity and an increase in the proliferation index 72 h after immunization (Fig. 4a-c). Approximately 80% of OVA_T-specific $CD8^+$ T cells divided for 7–9 generations in the OVA_T-FNs + Poly(I: C) group (Fig. S7c). The above results indicated that OVA_T-FNs + Poly(I: C) could consistently stimulated the proliferation of large numbers of OVA_T-specific $CD8^+$ T cells than the free peptide. Meanwhile, neither FNs nor FNs + Poly(I: C) were able to stimulate the proliferation of OVA_T-specific $CD8^+$ T cells. Therefore, in the subsequent experiments, these controls will no longer be included. Instead, the focus will shift to investigating whether FNs, as a carrier of neoantigen peptides, can enhance the induced antitumor immune response compared to free peptides.

The OVA_T-specific $CD8^+$ T-cell immune responses induced by OVA_T-FNs + Poly(I: C) were investigated 7 days after the second immunization (Fig. 4d). The

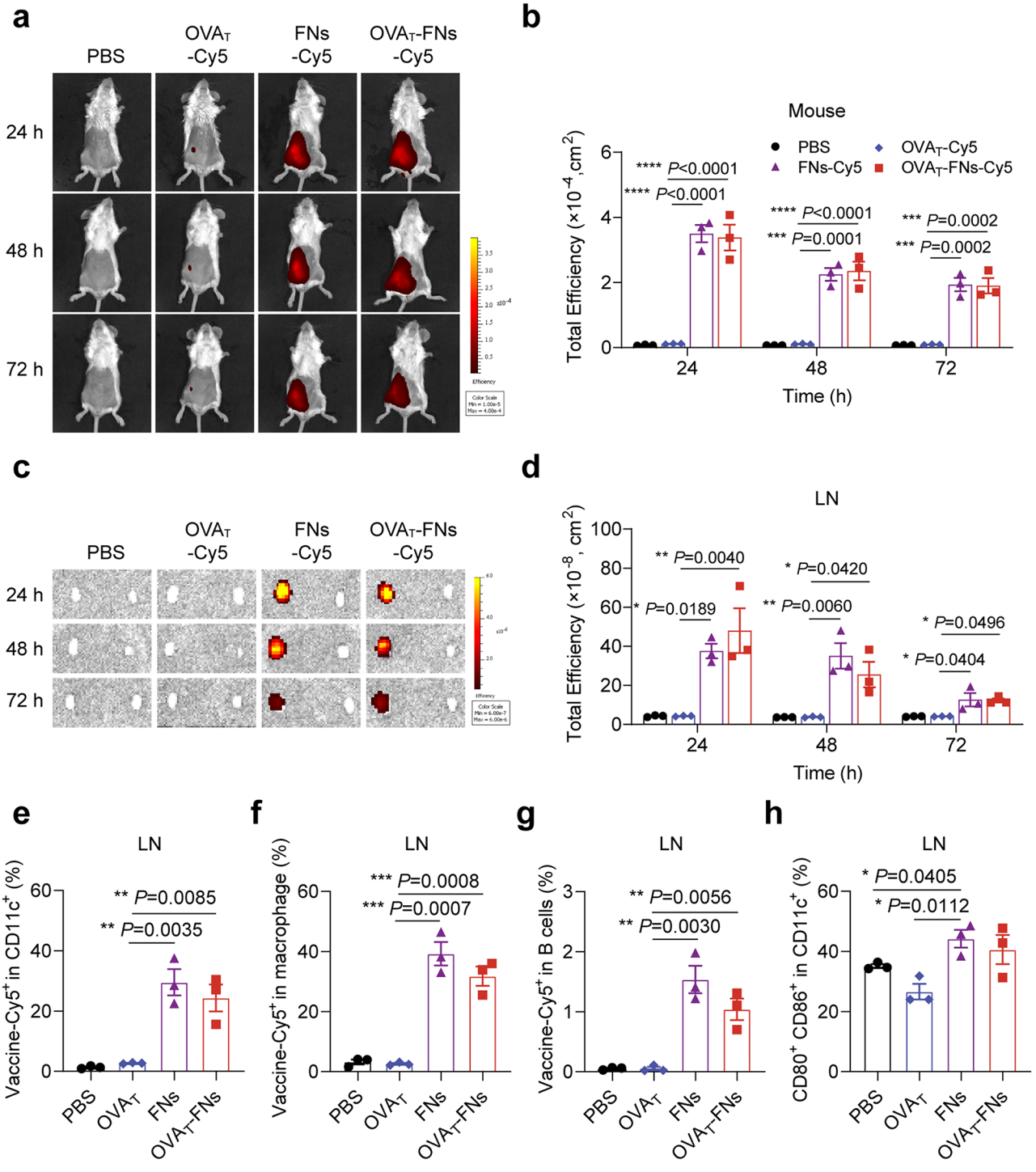

Fig. 3 OVA_T-FNs for lymph node targeting and were taken up by APCs in the lymph nodes. **a**, **b**, Live imaging of the location of OVA_T-FNs in vivo. BALB/c mice were subcutaneously administered in the left groin with 6 nmol Cy5-labeled vaccines. Fluorescence images (**a**) and total efficiency (**b**) at 24 h, 48 h, and 72 h after administration are shown ($n = 3$). **c**, **d**, Representative fluorescence images (**c**) and total efficiency (**d**) of lymph nodes. C57BL/6 mice were subcutaneously administered in the left groin with PBS or 6 nmol Cy5-labeled vaccine, and the lymph nodes were removed at 24 h, 48 h, and 72 h after administration ($n = 3$). **e-h**, Flow cytometry analysis of the frequencies of vaccine$^+$ cells among CD11c$^+$ DCs (**e**), macrophages (**f**) and B cells (**g**) and the frequency of CD80$^+$ CD86$^+$ CD11c$^+$ (**h**) cells in the lymph nodes ($n = 3$). **b**, **d-h**, Data are presented as the mean ± s.e.m. **b**, **d**, Statistical significance between the groups was assessed using one-way ANOVA. **e-h**, Statistical significance between the groups was assessed using two-tailed unpaired Student's *t* test. $^*P < 0.05$, $^{**}P < 0.01$, $^{***}P < 0.001$, $^{****}P < 0.0001$

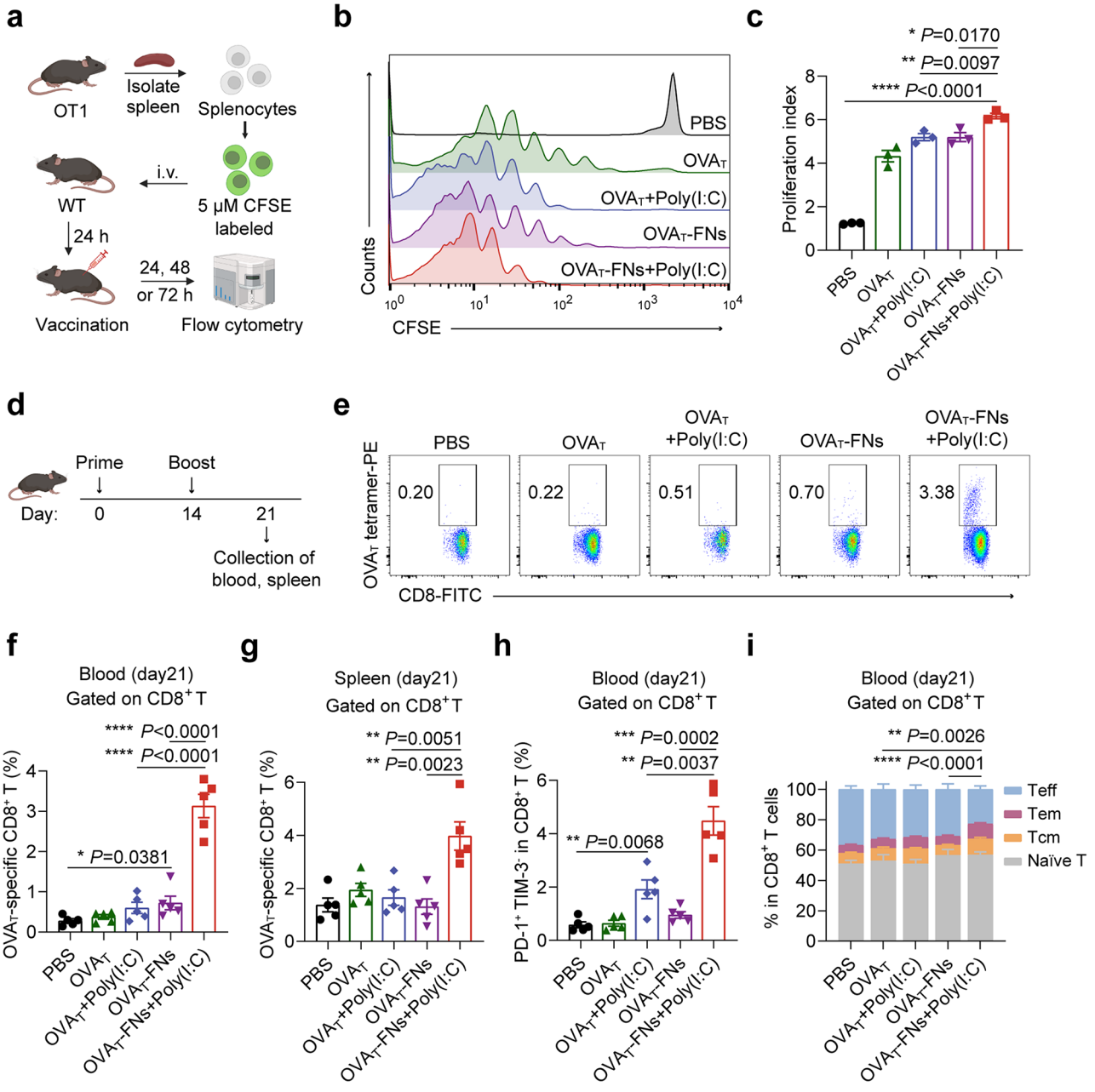

Fig. 4 Effect of OVA $_T$-FNs on the proliferation and production of OVA$_T$-specific CD8$^+$ T cells. **a**-**c**, Proliferation of OVA$_T$-specific CD8$^+$ T cells induced by OVA$_T$-FNs + Poly(I: C) in vivo. Schematic diagram of the experimental design (**a**), flow cytometry analysis data (**b**) and proliferation index (**c**) for the proliferation of CFSE-labeled OVA$_T$-specific CD8$^+$ T cells ($n = 3$). **d**, Schematic diagram for evaluating immune responses induced by OVA$_T$-FNs + Poly(I: C). **e-i**, C57BL/6 mice ($n = 5$) were vaccinated subcutaneously with OVA$_T$-FNs + Poly(I: C) or controls. Whole blood (**e**, **f**, **h**, **i**) and spleen (**g**) were collected on day 21. **e-g**, Flow cytometry analysis of the frequency of OVA$_T$-specific-CD8$^+$ T cells in the blood (**e**, **f**) and the spleen (**g**). **h**, Flow cytometry analysis of the frequency of PD-1$^+$ TIM-3$^-$ CD8$^+$ T cells in the blood. **i**, CD8$^+$ T cells were subdivided into CD62L$^+$ CD44$^-$ (gray, naïve T), CD62L$^+$ CD44$^+$ (yellow, Tcm), CD62L$^-$ CD44^{hi} (purple, Tem), and CD62L$^-$ CD44^{lo} (blue, Teff) subsets based on CD62L and CD44 expression. **c**, **f-i**, Data are presented as the mean ± s.e.m. Statistical significance between the groups was assessed using two-tailed unpaired Student's *t* test. *$P < 0.05$, **$P < 0.01$, ***$P < 0.001$, ****$P < 0.0001$

proportion of OVA$_T$-specific CD8$^+$ T cells in the peripheral blood of mice immunized with OVA$_T$-FNs + Poly(I: C) was significantly up-regulated compared with controls (Fig. 4e, f and Fig. S8). Moreover, the proportion of OVA$_T$-specific CD8$^+$ T cells in the spleen was also elevated in the OVA$_T$-FNs + Poly(I: C) group compared to the other groups (Fig. 4g). These results indicated that OVA$_T$-FNs prepared by fusing OVA$_T$ peptide with optimized ferritin to efficiently deliver the antigen peptide significantly enhanced CD8$^+$ T-cell immune responses.

Furthermore, the quality of triggered CD8$^+$ T-cell response is also an important determinant of the

therapeutic efficacy of tumor vaccines [47, 48]. To investigate the phenotype of $CD8^+$ T cells induced by OVA_T-FNs + Poly(I: C), we evaluated the levels of cell surface markers indicating activation, exhaustion, and dysfunction. 4% of $CD8^+$ T cells in the peripheral blood of mice immunized with OVA_T-FNs + Poly(I: C) expressed PD-1 but not TIM-3 (Fig. 4h), and a very limited number of cells expressed both PD-1 and TIM-3 (Fig. S9a, b) [49]. Based on the expression levels of CD44 and CD62L, approximately 25% of the total $CD8^+$ T cells were induced as central memory T cells (Tcm) and effector memory T cells (Tem) after immunized with OVA_T-FNs + Poly(I: C), which contribute to superior persistence and antitumor immunity (Fig. 4i and Fig. S9c) [50, 51]. In conclusion, OVA_T-FNs + Poly(I: C) induced a large number of OVA_T-specific $CD8^+$ T cells in vivo that maintained favorable early differentiation characteristics.

Enhancement of CTL responses by OVAT-FNs + poly(I: C)

Antigen-specific $CD8^+$ T cells generate strong CTL responses after a second exposure to the same antigen. To explore the level of CTL responses induced by OVA_T-FNs + Poly(I: C), we measured the levels of key effectors secreted by $CD8^+$ T cells after OVA_T peptide restimulation. As shown in Fig. 5a, b, after restimulation for 48 h, approximately 180 IFN-γ-secreting $CD8^+$ T cells were detected among 2×10^5 splenocytes from mice immunized with OVA_T-FNs + Poly(I: C). Similarly, the concentration of IFN-γ secreted by splenocytes was much higher in mice immunized with OVA_T-FNs + Poly(I: C) compared to those immunized with OVA_T and OVA_T-FNs (Fig. 5c). After restimulation with OVA_T peptide and Golgi plug for 6 h, the frequency of IFN-γ- secreting $CD8^+$ T cells was significantly elevated in the mice immunized with OVA_T-FNs + Poly(I: C) than in the other groups (Fig. 5d, e and Fig. S10). As mentioned above, comparable amounts of IFN-γ were detected in mice immunized with OVA_T+Poly(I: C) and OVA_T-FNs + Poly(I: C), as shown by ELISpot and ELISA. However, the flow cytometry results revealed that the frequency of IFN-γ secretion by $CD8^+$ T cells was significantly higher in the mice immunized with the OVA_T-FNs + Poly(I: C) than in the other groups. The possible reason might be that prolonged restimulation of splenocytes in ELISpot and ELISA may lead to a sustained accumulation of secreted IFN-γ around the cells. The level of Granzyme B, another important effector molecule, was also dramatically increased in mice immunized with OVA_T-FNs + Poly(I: C) (Fig. 5f).

To directly verify the cytotoxic function of OVA_T-specific $CD8^+$ T cells induced by OVA_T-FNs + Poly(I: C) in vivo, we performed a target cell lysis assay based on labeling with different concentrations of CFSE. The frequency of cells labelled with 5 μM and 0.5 μM CFSE in the spleen and lymph nodes were analyzed 18 h after the cell mixture was transferred to verify the killing efficiency of vaccine-induced $CD8^+$ T cells against target cells (Fig. 5g). The results showed that OVA_T-specific $CD8^+$ T cells induced by OVA_T-FNs + Poly(I: C) killed 80% of target cells, whereas those induced by OVA_T+Poly(I: C) killed only 60% of target cells (Fig. 5h, i and Fig. S11). Overall, the increased secretion of multiple effectors by OVA_T-specific $CD8^+$ T cells suggested that OVA_T-FNs + Poly(I: C) can induce robust CTL responses in vivo and can kill target cells specifically.

Growth inhibition of multiple primary tumors induced by OVAT-FNs + poly(I: C)

To further evaluate the antitumor immune responses induced by OVA_T-FNs + Poly(I: C) in vivo, we employed a variety of prophylactic tumor models to investigate the inhibition of tumor growth. C57BL/6 mice were immunized every 14 days and challenged with E.G7-OVA lymphoma cells 2 weeks after the third immunization. As demonstrated by the average growth curves and the individual tumor growth curves, compared with immunization with other control vaccines, immunization with OVA_T-FNs + Poly(I: C) significantly inhibited tumor growth. In addition, the tumors were isolated 16 days after implantation, and the tumor size was markedly smaller in the mice vaccinated with OVA_T-FNs + Poly(I: C) than in the other groups (Fig. 6a-d).

Next, the immune protection triggered by OVA_T-FNs + Poly(I: C) was explored in a highly immunogenic MC-38-OVA colon cancer model, and immunization with OVA_T-FNs + Poly(I: C) significantly inhibited tumor growth and prolonged survival. In addition, on day 60 after tumor implantation, a slightly palpable tumor was observed in one mouse in the OVA_T-FNs + Poly(I: C) group, while the other four tumors remained undetectable (Fig. 6e-g and Fig. S12a). Moreover, in the poorly immunogenic B16F10-OVA melanoma model, tumor growth was significantly controlled in mice immunized with OVA_T-FNs + Poly(I: C) (Fig. S12b, c). In all three different prophylactic tumor models, there was no weight loss in any of the immunized mice, suggesting that OVA_T-FNs + Poly(I: C) had no obvious side effects in vivo (Fig. S12d-f).

The safety of tumor vaccines is an important factor that must be evaluated in preclinical studies, so we assessed the side effects of OVA_T-FNs on cells or mice. In vitro, neither FNs nor OVA_T-FNs affected the viability of the mouse fibroblasts (3T3 cells), human fetal hepatocytes (LO2 cells), and mouse PBMCs, suggesting that FNs and OVA_T-FNs are not toxic to normal tissues, such as skin and liver, and to the immune system (Fig. 6h and Fig. S13a). In vivo, H&E staining data showed that mice immunized three times with OVA_T-FNs + Poly(I: C) did

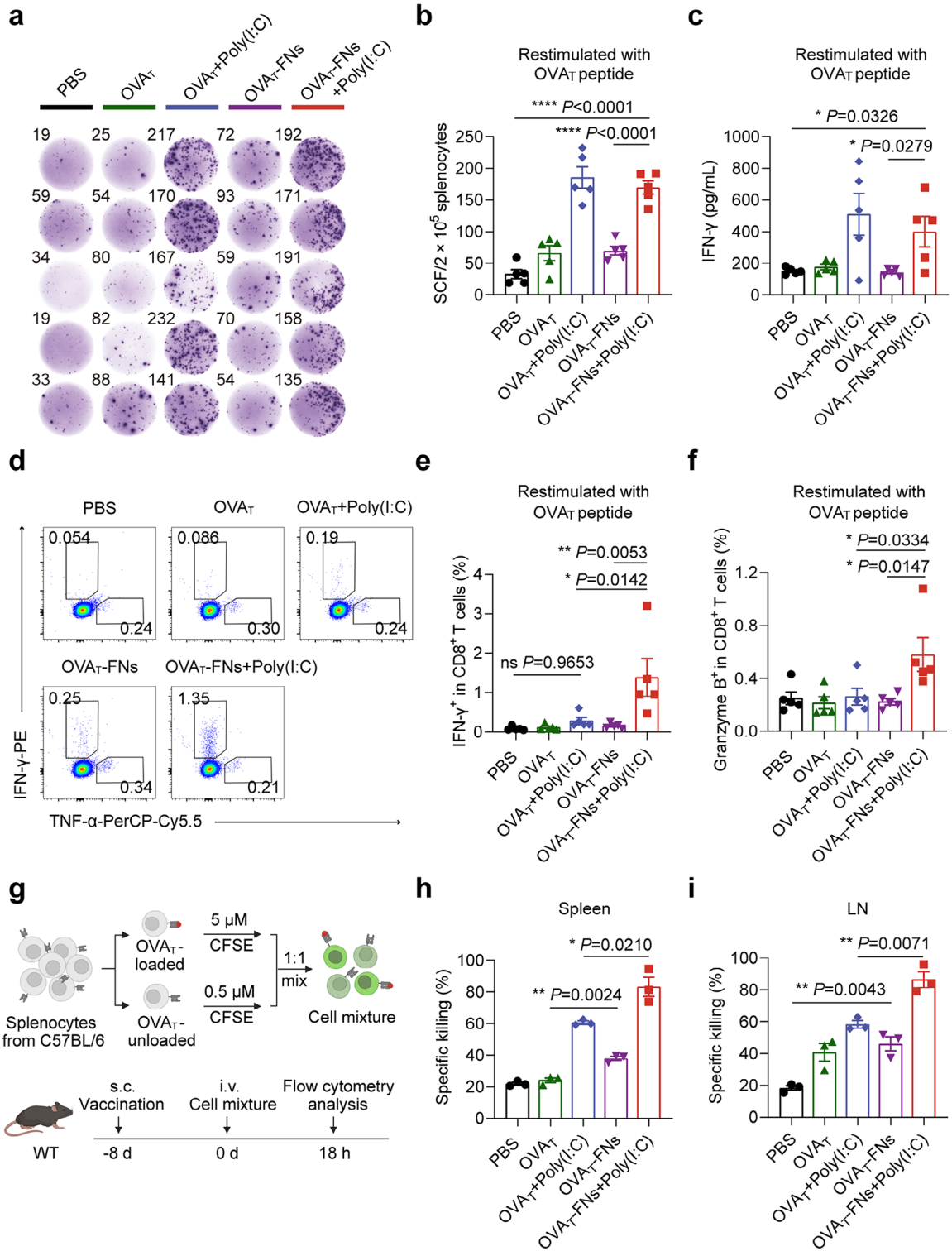

Fig. 5 OVA $_T$-FNs + Poly(I: C) for the elicitation of CTL responses. **a**, **b**, ELISpot of IFN-γ spot-forming cells in 2×10^5 splenocytes restimulated with OVA$_T$ peptide for 48 h on day 21 ($n = 5$). **c**, IFN-γ secretion in the supernatant of 2×10^5 splenocytes restimulated with OVA$_T$ peptide for 48 h, as measured by ELISA ($n = 5$). **d-f**, Flow cytometry data showing the frequencies of IFN-γ$^+$ (**d**, **e**) and Granzyme B$^+$ (**f**) CD8$^+$ T cells in the spleen on day 21. A total of 1×10^6 splenocytes were restimulated with OVA$_T$ peptide and a Golgi plug for 6 h ($n = 5$). **g-i**, CTL assay of OVA$_T$-specific CD8$^+$ T cells induced by OVA$_T$-FNs + Poly(I: C) in vivo ($n = 3$). Flow cytometry analysis of the frequency of OVA$_T$ loaded and unloaded splenocytes in the spleen (**h**) and lymph nodes (**i**). **b**, **c**, **e**, **f**, **h**, **i**, Representative data are shown as the mean ± s.e.m. The statistical significance between the groups was assessed using two-tailed unpaired Student's *t* test (**b**, **c**, **h**, **i**) and one-way ANOVA (**e**, **f**). *$P < 0.05$, **$P < 0.01$, ***$P < 0.001$, ****$P < 0.0001$

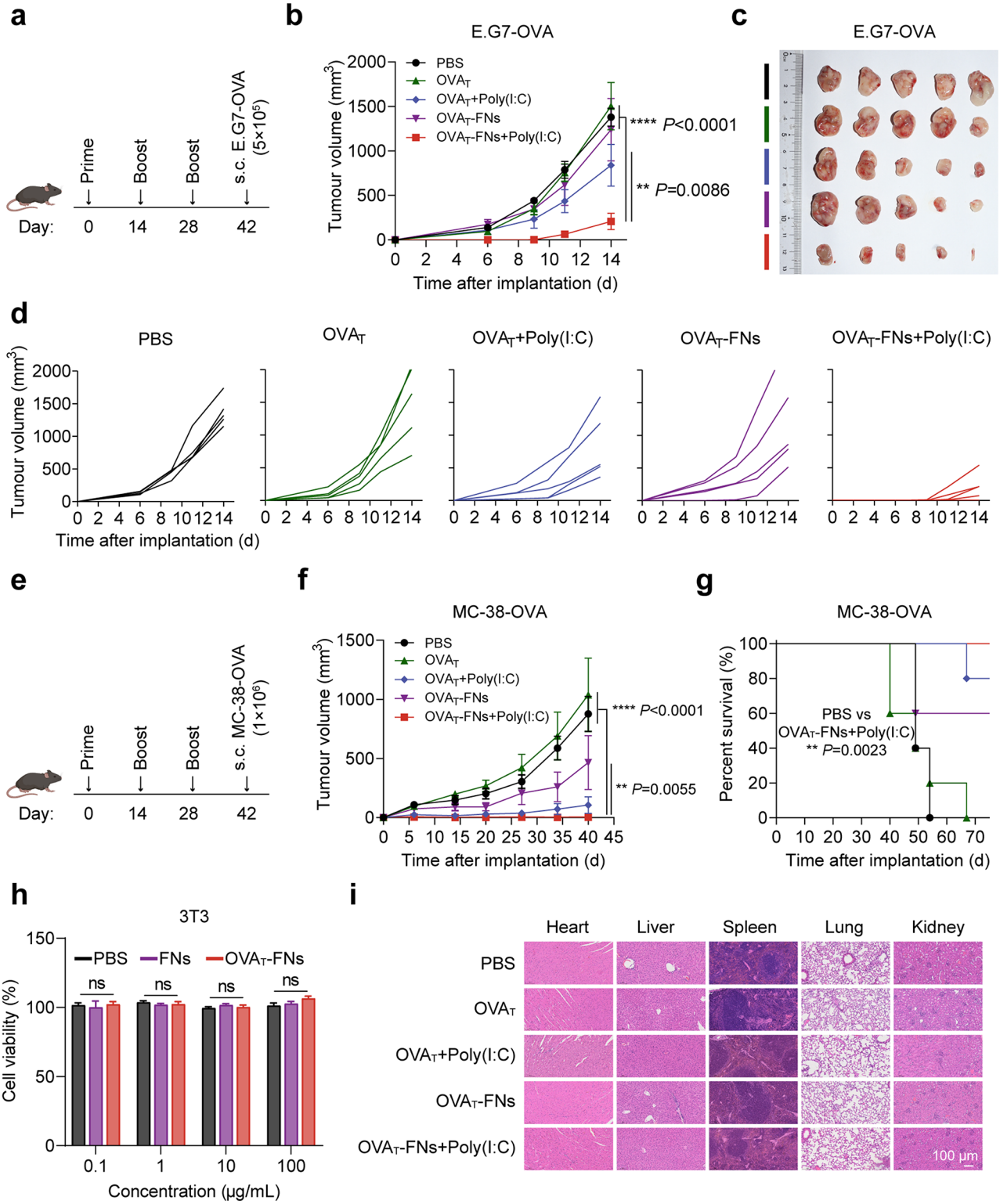

Fig. 6 OVA $_T$-FNs + Poly(I: C) inhibited tumor growth and are nontoxic. **a**-**d**, The prophylactic effects of OVA$_T$-FNs + Poly(I: C) against E.G7-OVA tumors ($n = 5$). Schematic illustration of the experimental design (**a**), average tumor growth curves (**b**) and tumor size on day 16 (**c**) are presented. **d**, Individual tumor growth curves of mice vaccinated with PBS (black), OVA$_T$ (green), OVA$_T$+Poly(I: C) (blue), OVA$_T$-FNs (purple) and OVA$_T$-FNs + Poly(I: C) (red) are shown. **e**-**g**, The prophylactic effects of OVA$_T$-FNs + Poly(I: C) against MC-38-OVA colon tumors ($n = 5$). Schematic illustration of the experimental design (**e**), average tumor growth curves (**f**) and survival curves (**g**) are shown. **h**, **i**, Biosafety assessment of OVA$_T$-FNs in vitro (**h**) and in vivo (**i**). **h**, Safety of FNs and OVA$_T$-FNs on mouse fibroblast 3T3 cells was assessed by CCK-8 assay ($n = 3$). **i**, Representative H&E-stained sections of the heart, liver, spleen, lung and kidney. Scale bar, 100 μm. **b**, **f**, **h**, Data are presented as the mean ± s.e.m. The statistical significance of differences between the groups was assessed using two-way ANOVA (**b**, **f**) and one-way ANOVA (**h**). **g**, Statistics were assessed by log rank test. $^*P < 0.05$, $^{**}P < 0.01$, $^{***}P < 0.001$, $^{****}P < 0.0001$

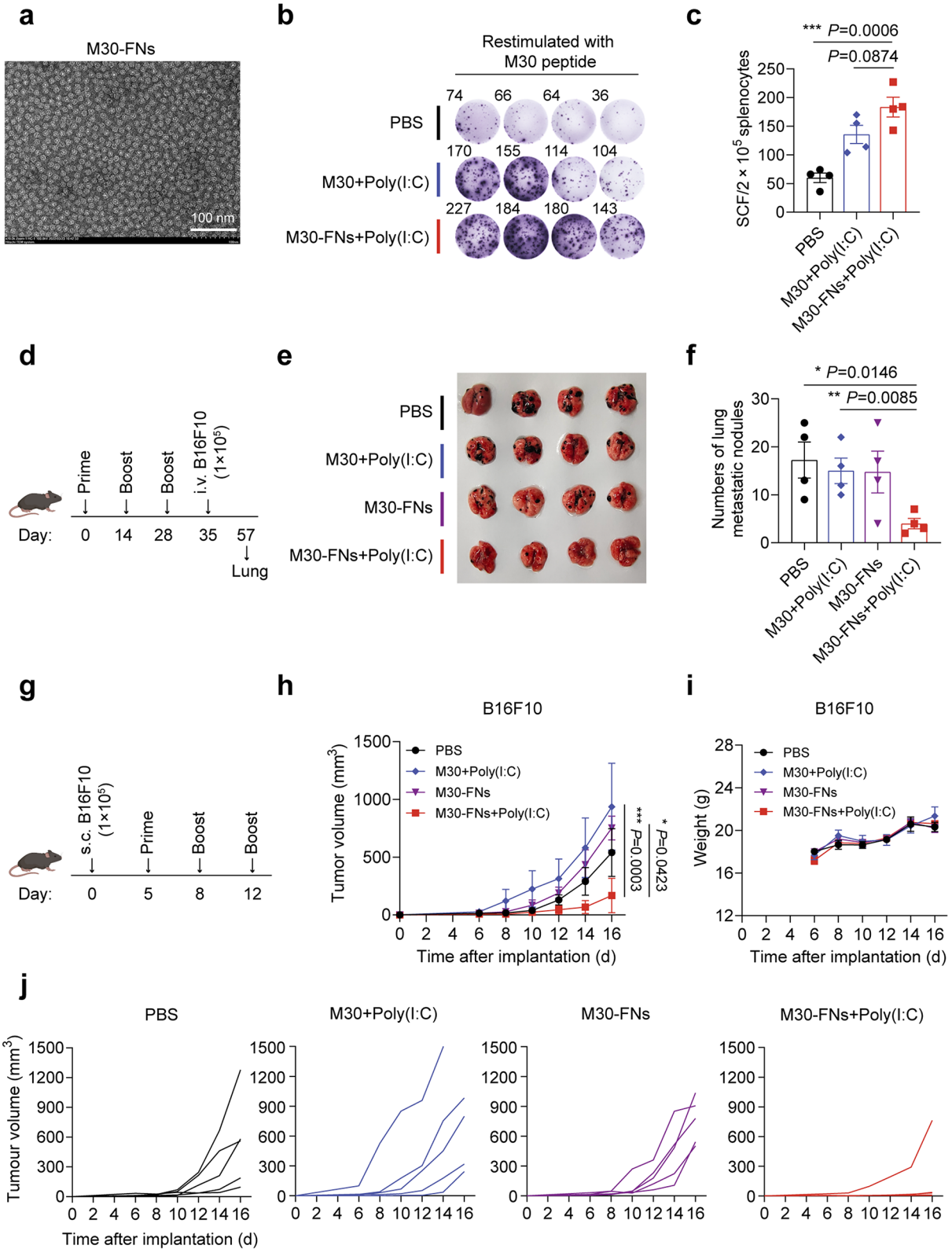

Fig. 7 (See legend on next page.)

(See figure on previous page.)

Fig. 7 Neoantigen-based M30-FNs + Poly(I: C) controlled the metastasis and growth of melanoma. **a**, TEM image of M30-FNs stained with 1% uranyl acetate. Scale bar, 100 nm. **b**, **c**, ELISpot of IFN-γ spot-forming cells in 2×10^5 splenocytes restimulated with M30 peptide ($n=4$). C57BL/6 mice were immunized with M30-FNs + Poly(I: C) on days 0 and 14, and the spleens were removed on day 21. **d-f**, The antitumor capacity of M30-FNs + Poly(I: C) in a prophylactic metastatic B16F10 melanoma model ($n=4$). A schematic illustration of the experimental design (**d**), pictures of the lungs (**e**) and the number of metastatic lung nodules (**f**) are shown. **g-j**, Antitumor therapeutic effects of M30-specific $CD8^+$ T cells induced by M30-FNs + Poly(I: C) against B16F10 tumors ($n=5$). Schematic illustration of the experimental design (**g**), average tumor growth curves (**h**), body weights (**i**) and individual tumor growth curves (**j**) are shown. **c**, **f**, **h**, **i**, Data are presented as the mean ± s.e.m. **c**, **f**, Statistical significance between the groups was assessed using a two-tailed unpaired Student's *t* test. **h**, **i**, Statistical significance between the groups was assessed using two-way ANOVA. $^*P<0.05$, $^{**}P<0.01$, $^{***}P<0.001$, $^{****}P<0.0001$

not exhibit damage to various tissues and organs (Fig. 6i). The expression of molecules associated with liver and kidney impairment were also not abnormally elevated in the serum (Fig. S13b). The above results indicated that OVA_T-FNs have satisfactory biosafety and do not cause hepatotoxicity, nephrotoxicity or pathological damage in vivo. Taken together, these results demonstrated that vaccination with OVA_T-FNs + Poly(I: C) not only significantly inhibit the growth of a wide range of tumors but also have a favorable safety profile.

M30-FNs + poly(I: C) showed significant efficacy in both metastatic and primary tumor-bearing models

We demonstrated that the delivery of the model antigen peptide OVA_T using optimized ferritin as a vaccine carrier significantly inhibited tumor growth. Next, we explored whether the fusion of neoantigens with optimized ferritin could also induce robust immune responses and inhibit tumor growth. M30-FNs were prepared by fusing M30, a B16F10 melanoma neoantigen, to the N-terminus of optimized ferritin [7]. SDS-PAGE image demonstrated that high-purity M30-FNs were obtained (Fig. S14). TEM image showed that M30-FNs self-assembled into homogeneous particles with a particle size of 12 nm (Fig. 7a). Splenocytes from mice immunized with M30-FNs + Poly(I: C) for 3 times were restimulated with the M30 peptide, and IFN-γ secretion was detected by ELISpot. The results showed more IFN-γ was secreted by 2×10^5 splenocytes from mice immunized with M30-FNs + Poly(I: C) than those immunized with M30 + Poly(I: C) (Fig. 7b, c).

The highly metastatic property of melanoma is one of the major causes of death in melanoma patients. The 5-year survival rate of primary melanoma patients is 99%, but that of metastatic melanoma patients is only 27% [52]. We therefore explored whether the neoantigen-FNs delivery system could function similarly in a metastatic tumor model. B16F10 cells were injected intravenously 7 days after the last immunization, and the lungs were removed 22 days after the injection to count the number of lung metastases (Fig. 7d). The numbers of metastatic foci were significantly reduced after immunization with M30-FNs + Poly(I: C) compared to approximately 15 metastatic foci that detected in each of the other groups (Fig. 7e, f). In addition, the area of lung tumor invasion was significantly reduced in mice immunized with M30-FNs + Poly(I: C) (Fig. S15). These results showed that T-cell immune responses induced by a neoantigen-FNs vaccine corresponding to B16F10 melanoma significantly inhibited tumor metastasis to the lungs.

Currently, personalized therapeutic tumor vaccines are being investigated extensively in the clinic [53]. We next explored the ability of M30-FNs + Poly(I: C) to induce regression of established tumors. C57BL/6 mice were subcutaneously implanted with B16F10 cells and then immunized 3 times on days 5, 8, and 12 (Fig. 7g). M30-FNs + Poly(I: C) significantly controlled tumor growth and had no effect on body weight compared to that in mice vaccinated with various other controls (Fig. 7h, i). On day 16, only 1 of the 5 mice showed visible tumors (Fig. 7j). These data suggested that neoantigen-FNs vaccine induce robust immune responses, significantly inhibit tumor metastasis, and promote regression of established tumors.

Discussion

Although tumor neoantigen peptide vaccines have achieved remarkable results in the treatment of solid tumors, it is clear that low immunogenicity, poor lymph node targeting, and insufficient immune responses remain major obstacles [11, 54, 55]. In this study, we developed a tumor neoantigen peptide delivery system based on ferritin nanoparticles (neoantigen-FNs), which significantly enhanced the proportion and function of antigen-specific $CD8^+$ T cells in vivo compared to free peptides. The neoantigen-FNs vaccine remarkably inhibited tumor growth and metastasis in a variety of prophylactic, B16F10 metastatic, and B16F10 therapeutic models and did not cause in vivo toxicity in mice with a favorable safety profile.

The homogeneity, stability and biosafety of therapeutic tumor vaccines are crucial for their clinical translation [40]. In this study, recombinant OVA_T-FNs prepared by fusion expression self-assembled into well-homogenized spherical particles with particle sizes of approximately 12 nm, similar to the natural structure of ferritin nanoparticles. Moreover, the structural properties of OVA_T-FNs did not change when they were heated at 4 °C for 7 days or even at 65 °C for 10 min. Besides the good thermal stability, OVA_T-FNs have excellent dispersion stability without aggregation. In addition, OVA_T-FNs had no effect on the viability of the mouse fibroblasts

3T3 cells, human fetal hepatocytes LO2 cells, and mouse PBMCs in vitro. In vivo, OVA_T-FNs also did not cause organ damage or serotoxicity, and there was no weight loss in the immunized mice, which suggested that the neoantigen-FNs peptide delivery system has good biosafety and has great potential to be applied in the clinic.

The antitumor effects of tumor vaccines depend on the uptake of antigens by APCs and their presentation to $CD8^+$ T cells in lymph nodes. Therefore, effective delivery of tumor vaccines to lymph nodes to increase the probability of contact with APCs would facilitate the activation of antitumor immune responses [56]. A well-established strategy to promote direct lymph node targeting is to design vaccines in particle form, and the size of particles has a significant impact on effective lymph node targeting [45]. OVA_T-FNs are spherical particles with a particle size of 12 nm, which strongly facilitates their localization in lymph nodes. The results of ex vivo lymph node imaging showed that OVA_T-FNs could drainage to and reside in lymph nodes, where they were then taken up by APCs, inducing the activation of DCs. Zhehui Qu et al. showed that *H. pylori*-derived recombinant ferritin nanoparticles RFNps bind to the TLR4 receptor of BMDCs and activate the NF-κB signaling pathway, thereby inducing the activation and maturation of BMDCs. This suggests that FNs themselves can be recognized and taken up by DCs as PAMPs, while FNs can not only act as an antigen peptide carrier but also as an immune adjuvant to activate more robust immune responses [57].

In clinical trials, failure to elicit effective antigen-specific T-cell responses in patients is a major obstacle for tumor neoantigen peptide vaccines [11]. Fusion of OVA_T peptides with FNs to enhance the immunogenicity and lymph node targeting of OVA_T peptides significantly increased the frequency of OVA_T-specific $CD8^+$ T cells in the peripheral blood and spleen. Moreover, not only the quantity but also the quality of OVA_T-specific $CD8^+$ T cells was been improved after OVA_T-FNs + Poly(I: C) treatment. We examined the expression levels of $CD8^+$ T-cell surface markers in the peripheral blood and showed that OVA_T-FNs + Poly(I: C) induced functional PD-1^+ TIM-3^- rather than exhausted $CD8^+$ T cells. In addition, approximately 25% of the total $CD8^+$ T cells were Tcm and Tem cells after immunized with OVA_T-FNs + Poly(I: C), which is also consistent with the more significant inhibition of tumor growth. Various results have confirmed that these $CD8^+$ T cells can secrete large amounts of effectors, such as IFN-γ and Granzyme B, thereby significantly inducing the lysis of target cells.

In various prophylactic tumor models, OVA_T-FNs + Poly(I: C) prepared based on the model antigen significantly inhibited tumor growth, suggesting that the use of FNs as an antigen delivery vehicle can dramatically enhance the antitumor efficacy of peptide vaccines. Moreover, melanoma is a highly malignant and extremely metastatic tumor, and the antitumor immune responses induced by M30-FNs + Poly(I: C), prepared by fusion of the neoantigen, also significantly inhibited melanoma metastasis to the lungs. Similarly, for established melanoma, M30-FNs + Poly(I: C) likewise induced tumor regression. The above results suggested that the use of FNs as delivery vectors for mutation-derived neoantigens, which are less effective in the clinic, could also significantly enhance tumor suppression.

Conclusions

We have developed an excellent platform for tumor neoantigen delivery, FNs, which are not only homogeneous in terms of particle size and structural stability, but also highly biocompatible. Fusion with FNs significantly enhanced the immunogenicity of antigen peptides and induced the activation and maturation of APCs. Notably, neoantigen-FNs effectively targeted lymph nodes, activated a large number of early-differentiated antigen-specific $CD8^+$ T cells in vivo, and exhibited a striking ability to kill target cells. Both activated model antigen- and neoantigen-specific immune responses significantly inhibit tumor growth. In conclusion, FNs can be used as ideal neoantigen delivery platforms to further improve the effectiveness of neoantigen peptide vaccines, which not only broadens the road of neoantigen peptide vaccine delivery vehicles but also has great potential for clinical application.

Abbreviations

Neoantigen	Ferritin nanoparticles (neoantigen-FNs)
FDA	Food and Drug Administration
CTL	Cytotoxic T lymphocyte
VLPs	Virus-like particles
hFTN	Human ferritin heavy chain
OVA^T-FNs	OVA^T-ferritin nanoparticles
APCs	Antigen presenting cells
WT	Wild-type
ATCC	American Type Culture Collection
FBS	Fetal bovine serum
HI-FBS	Heat-inactivated fetal bovine serum
E. coli	*Escherichia coli*
IPTG	Isopropyl *β*-D-1-thiogalactopyranoside
MWCO	Molecular weight cutoff
DLS	Dynamic light scattering
BMDCs	Bone marrow-derived dendritic cells
ELISA	Enzyme-Linked Immunosorbent Assay
ELISpot	Enzyme-Linked Immunospot
H&E	Hematoxylin and eosin
LN	Lymph node
Th1	T helper 1
Tem	Effector memory T
Tcm	Central memory T
TEM	Transmission electron microscopy
AST	Aspartate aminotransferase
ALT	Alanine aminotransferase
BUN	Blood urea nitrogen
CRE	Creatinine

Supplementary Information

The online version contains supplementary material available at https://doi.org/10.1186/s12951-024-02837-2.

Supplementary Material 1

Acknowledgements
The authors acknowledge support from the National Key R&D Program of China (No. 2022YFC2304202) and the National Natural Science Foundation of China (No.82073341). We sincerely appreciate the help and guidance of teachers Yajuan Wan, Rui Wang, Ruming Liu, Li Jiao, Di An and Ying Zhou from the Instrumentation Platform of Nankai University, as well as Xiaomin Su and Yanfang Chen from the Animal Experiment Center of Nankai University.

Author contributions
WZ, SL, KS, and FW conceived and designed the experiments; WZ, SL, ZS, HZ, KS, YD, LZ, QT, and JH performed all the experiments; WZ, SL, ZS, LZ, and HZ analyzed the data obtained; WZ, SL, and FW wrote the manuscript.

Funding
This research was supported by the National Key R&D Program of China (No. 2022YFC2304202) and the National Natural Science Foundation of China (No.82073341).

Data availability
No datasets were generated or analysed during the current study.

Declarations

Ethics approval and consent to participate
All of the animal experimental manipulations included in this study were approved by the policies and guidelines of the Animal Ethics Committee of Nankai University (2022-SYDWLL-000639).

Consent for publication
Not applicable.

Competing interests
The authors declare no competing interests.

Author details
[1]State Key Laboratory of Medicinal Chemical Biology, Tianjin Key Laboratory of Protein Sciences, Cancer Biology Center, College of Life Sciences, Nankai University, Tianjin 300071, PR China
[2]School of Medicine, Nankai University, Tianjin 300071, PR China
[3]People's Hospital of Tianjin, Tianjin 300180, PR China
[4]Nankai International Advanced Research Institute (SHENZHEN FUTIAN), Shenzhen 518045, PR China

Received: 28 June 2024 / Accepted: 5 September 2024
Published online: 14 September 2024

References

1. Saxena M, van der Burg SH, Melief CJM, Bhardwaj N. Therapeutic cancer vaccines. Nat Rev Cancer. 2021;21(6):360–78.
2. Weber JS, Carlino MS, Khattak A, Meniawy T, Ansstas G, Taylor MH, et al. Individualised neoantigen therapy mRNA-4157 (V940) plus pembrolizumab versus pembrolizumab monotherapy in resected melanoma (KEYNOTE-942): a randomised, phase 2b study. Lancet. 2024;403(10427):632–44.
3. Pant S, Wainberg ZA, Weekes CD, Furqan M, Kasi PM, Devoe CE, et al. Lymph-node-targeted, mKRAS-specific amphiphile vaccine in pancreatic and colorectal cancer: the phase 1 AMPLIFY-201 trial. Nat Med. 2024;30(2):531–42.
4. Kantoff PW, Higano CS, Shore ND, Berger ER, Small EJ, Penson DF, et al. Sipuleucel-T immunotherapy for castration-resistant prostate cancer. N Engl J Med. 2010;363(5):411–22.
5. Cheever MA, Higano CS. PROVENGE (Sipuleucel-T) in prostate cancer: the first FDA-approved therapeutic cancer vaccine. Clin Cancer Res. 2011;17(11):3520–6.
6. Yadav M, Jhunjhunwala S, Phung QT, Lupardus P, Tanguay J, Bumbaca S, et al. Predicting immunogenic tumour mutations by combining mass spectrometry and exome sequencing. Nature. 2014;515(7528):572–6.
7. Kreiter S, Vormehr M, van de Roemer N, Diken M, Lower M, Diekmann J, et al. Mutant MHC class II epitopes drive therapeutic immune responses to cancer. Nature. 2015;520(7549):692–6.
8. Lang F, Schrors B, Lower M, Tureci O, Sahin U. Identification of neoantigens for individualized therapeutic cancer vaccines. Nat Rev Drug Discov. 2022;21(4):261–82.
9. Ott PA, Hu Z, Keskin DB, Shukla SA, Sun J, Bozym DJ, et al. An immunogenic personal neoantigen vaccine for patients with melanoma. Nature. 2017;547(7662):217–21.
10. Awad MM, Govindan R, Balogh KN, Spigel DR, Garon EB, Bushway ME, et al. Personalized neoantigen vaccine NEO-PV-01 with chemotherapy and anti-PD-1 as first-line treatment for non-squamous non-small cell lung cancer. Cancer Cell. 2022;40(9):1010–e2611.
11. Lybaert L, Lefever S, Fant B, Smits E, De Geest B, Breckpot K, et al. Challenges in neoantigen-directed therapeutics. Cancer Cell. 2023;41(1):15–40.
12. Katsikis PD, Ishii KJ, Schliehe C. Challenges in developing personalized neoantigen cancer vaccines. Nat Rev Immunol. 2024;24(3):213–27.
13. Xu J, Lv J, Zhuang Q, Yang Z, Cao Z, Xu L, et al. A general strategy towards personalized nanovaccines based on fluoropolymers for post-surgical cancer immunotherapy. Nat Nanotechnol. 2020;15(12):1043–52.
14. Kim J, Li WA, Choi Y, Lewin SA, Verbeke CS, Dranoff G, et al. Injectable, spontaneously assembling, inorganic scaffolds modulate immune cells in vivo and increase vaccine efficacy. Nat Biotechnol. 2015;33(1):64–72.
15. Affandi AJ, Grabowska J, Olesek K, Lopez Venegas M, Barbaria A, Rodriguez E, et al. Selective tumor antigen vaccine delivery to human CD169(+) antigen-presenting cells using ganglioside-liposomes. Proc Natl Acad Sci U S A. 2020;117(44):27528–39.
16. Liu J, Liew SS, Wang J, Pu K. Bioinspired and Biomimetic Delivery platforms for Cancer vaccines. Adv Mater. 2022;34(1):e2103790.
17. Nooraei S, Bahrulolum H, Hoseini ZS, Katalani C, Hajizade A, Easton AJ, et al. Virus-like particles: preparation, immunogenicity and their roles as nanovaccines and drug nanocarriers. J Nanobiotechnol. 2021;19(1):59.
18. Chen H, Tan X, Han X, Ma L, Dai H, Fu Y, et al. Ferritin nanocage based delivery vehicles: from single-, co- to compartmentalized- encapsulation of bioactive or nutraceutical compounds. Biotechnol Adv. 2022;61:108037.
19. Kim SA, Lee Y, Ko Y, Kim S, Kim GB, Lee NK, et al. Protein-based nanocages for vaccine development. J Control Release. 2023;353:767–91.
20. Jiang J, Xie D, Zhang W, Xiao G, Wen J. Fusion of Hsp70 to Mage-a1 enhances the potency of vaccine-specific immune responses. J Transl Med. 2013;11:300.
21. Cheng K, Du T, Li Y, Qi Y, Min H, Wang Y, et al. Dual-Antigen-Loaded Hepatitis B Virus Core Antigen Virus-like particles stimulate efficient immunotherapy against Melanoma. ACS Appl Mater Interfaces. 2020;12(48):53682–90.
22. Li W, Jing Z, Wang S, Li Q, Xing Y, Shi H, et al. P22 virus-like particles as an effective antigen delivery nanoplatform for cancer immunotherapy. Biomaterials. 2021;271:120726.
23. Trevaskis NL, Kaminskas LM, Porter CJ. From sewer to saviour - targeting the lymphatic system to promote drug exposure and activity. Nat Rev Drug Discov. 2015;14(11):781–803.
24. Lee BR, Ko HK, Ryu JH, Ahn KY, Lee YH, Oh SJ, et al. Engineered Human Ferritin nanoparticles for Direct Delivery of Tumor antigens to Lymph Node and Cancer Immunotherapy. Sci Rep. 2016;6:35182.
25. Cho KJ, Shin HJ, Lee JH, Kim KJ, Park SS, Lee Y, et al. The crystal structure of ferritin from Helicobacter pylori reveals unusual conformational changes for iron uptake. J Mol Biol. 2009;390(1):83–98.
26. Rodrigues MQ, Alves PM, Roldao A. Functionalizing ferritin nanoparticles for Vaccine Development. Pharmaceutics. 2021;13(10).
27. Kanekiyo M, Wei CJ, Yassine HM, McTamney PM, Boyington JC, Whittle JR, et al. Self-assembling influenza nanoparticle vaccines elicit broadly neutralizing H1N1 antibodies. Nature. 2013;499(7456):102–6.
28. Li Z, Cui K, Wang H, Liu F, Huang K, Duan Z, et al. A milk-based self-assemble rotavirus VP6-ferritin nanoparticle vaccine elicited protection against the viral infection. J Nanobiotechnol. 2019;17(1):13.
29. Saunders KO, Lee E, Parks R, Martinez DR, Li D, Chen H, et al. Neutralizing antibody vaccine for pandemic and pre-emergent coronaviruses. Nature. 2021;594(7864):553–9.

30. Joyce MG, Chen WH, Sankhala RS, Hajduczki A, Thomas PV, Choe M, et al. SARS-CoV-2 ferritin nanoparticle vaccines elicit broad SARS coronavirus immunogenicity. Cell Rep. 2021;37(12):110143.
31. Mu Z, Wiehe K, Saunders KO, Henderson R, Cain DW, Parks R, et al. mRNA-encoded HIV-1 Env trimer ferritin nanoparticles induce monoclonal antibodies that neutralize heterologous HIV-1 isolates in mice. Cell Rep. 2022;38(11):110514.
32. Vu MN, Pilkington EH, Lee WS, Tan HX, Davis TP, Truong NP, et al. Engineered Ferritin Nanoparticle vaccines Enable Rapid screening of antibody functionalization to Boost Immune responses. Adv Healthc Mater. 2023;12(17):e2202595.
33. Houser KV, Chen GL, Carter C, Crank MC, Nguyen TA, Burgos Florez MC, et al. Safety and immunogenicity of a ferritin nanoparticle H2 influenza vaccine in healthy adults: a phase 1 trial. Nat Med. 2022;28(2):383–91.
34. Ober Shepherd BL, Scott PT, Hutter JN, Lee C, McCauley MD, Guzman I, et al. SARS-CoV-2 recombinant spike ferritin nanoparticle vaccine adjuvanted with Army Liposome Formulation containing monophosphoryl lipid A and QS-21: a phase 1, randomised, double-blind, placebo-controlled, first-in-human clinical trial. Lancet Microbe. 2024;5(6):e581–93.
35. Han JA, Kang YJ, Shin C, Ra JS, Shin HH, Hong SY, et al. Ferritin protein cage nanoparticles as versatile antigen delivery nanoplatforms for dendritic cell (DC)-based vaccine development. Nanomedicine. 2014;10(3):561–9.
36. Wang W, Liu Z, Zhou X, Guo Z, Zhang J, Zhu P, et al. Ferritin nanoparticle-based SpyTag/SpyCatcher-enabled click vaccine for tumor immunotherapy. Nanomedicine. 2019;16:69–78.
37. Badrinath S, Dellacherie MO, Li A, Zheng S, Zhang X, Sobral M, et al. A vaccine targeting resistant tumours by dual T cell plus NK cell attack. Nature. 2022;606(7916):992–8.
38. Kim D, Lai CJ, Cha I, Kang S, Yang WS, Choi Y, et al. SFTSV Gn-Head mRNA vaccine confers efficient protection against lethal viral challenge. J Med Virol. 2023;95(11):e29203.
39. Jing Z, Wang S, Xu K, Tang Q, Li W, Zheng W, et al. A potent Micron Neoantigen Tumor Vaccine GP-Neoantigen induces Robust Antitumor activity in multiple tumor models. Adv Sci (Weinh). 2022;9(24):e2201496.
40. Shi J, Kantoff PW, Wooster R, Farokhzad OC. Cancer nanomedicine: progress, challenges and opportunities. Nat Rev Cancer. 2017;17(1):20–37.
41. Wculek SK, Cueto FJ, Mujal AM, Melero I, Krummel MF, Sancho D. Dendritic cells in cancer immunology and immunotherapy. Nat Rev Immunol. 2020;20(1):7–24.
42. Curtsinger JM, Mescher MF. Inflammatory cytokines as a third signal for T cell activation. Curr Opin Immunol. 2010;22(3):333–40.
43. Jin SM, Yoo YJ, Shin HS, Kim S, Lee SN, Lee CH, et al. A nanoadjuvant that dynamically coordinates innate immune stimuli activation enhances cancer immunotherapy and reduces immune cell exhaustion. Nat Nanotechnol. 2023;18(4):390–402.
44. Wang Q, Wang Z, Sun X, Jiang Q, Sun B, He Z, et al. Lymph node-targeting nanovaccines for cancer immunotherapy. J Control Release. 2022;351:102–22.
45. Wang Y, Wang H. Lymph node targeting for immunotherapy. Immunooncol Technol. 2023;20:100395.
46. Hu Z, Leet DE, Allesoe RL, Oliveira G, Li S, Luoma AM, et al. Personal neoantigen vaccines induce persistent memory T cell responses and epitope spreading in patients with melanoma. Nat Med. 2021;27(3):515–25.
47. Oliveira G, Stromhaug K, Klaeger S, Kula T, Frederick DT, Le PM, et al. Phenotype, specificity and avidity of antitumour CD8(+) T cells in melanoma. Nature. 2021;596(7870):119–25.
48. Philip M, Schietinger A. CD8(+) T cell differentiation and dysfunction in cancer. Nat Rev Immunol. 2022;22(4):209–23.
49. Baharom F, Ramirez-Valdez RA, Tobin KKS, Yamane H, Dutertre CA, Khalilnezhad A, et al. Intravenous nanoparticle vaccination generates stem-like TCF1(+) neoantigen-specific CD8(+) T cells. Nat Immunol. 2021;22(1):41–52.
50. Sallusto F, Lenig D, Forster R, Lipp M, Lanzavecchia A. Two subsets of memory T lymphocytes with distinct homing potentials and effector functions. Nature. 1999;401(6754):708–12.
51. Liu Q, Sun Z, Chen L, Memory. T cells: strategies for optimizing tumor immunotherapy. Protein Cell. 2020;11(8):549–64.
52. Eddy K, Shah R, Chen S. Decoding Melanoma Development and Progression: identification of therapeutic vulnerabilities. Front Oncol. 2020;10:626129.
53. Lin MJ, Svensson-Arvelund J, Lubitz GS, Marabelle A, Melero I, Brown BD, et al. Cancer vaccines: the next immunotherapy frontier. Nat Cancer. 2022;3(8):911–26.
54. Blass E, Ott PA. Advances in the development of personalized neoantigen-based therapeutic cancer vaccines. Nat Rev Clin Oncol. 2021;18(4):215–29.
55. Sahin U, Tureci O. Personalized vaccines for cancer immunotherapy. Science. 2018;359(6382):1355–60.
56. Liu H, Moynihan KD, Zheng Y, Szeto GL, Li AV, Huang B, et al. Structure-based programming of lymph-node targeting in molecular vaccines. Nature. 2014;507(7493):519–22.
57. Qu Z, Guo Y, Li M, Cao C, Wang J, Gao M. Recombinant ferritin nanoparticles can induce dendritic cell maturation through TLR4/NF-κB pathway. Biotechnol Lett. 2020;42(12):2489–500.

Publisher's note